Rapid and Portable Detection of Food Adulteration Using Paper-based SERS Swabs

A thesis submitted

for the degree of

Master of Technology (Research)

in the Faculty of Engineering

by

Aditya Kumar

Department of Chemical Engineering

Indian Institute of Science

Bengaluru 560012 (India)

March 2019

Declaration

I certify that I wrote the thesis, and in writing the thesis,

1 experimental data collected/simulation results obtained by me have been presented without any bias, modifications, or alterations, and can be obtained by others using the information provided in the report

2 I have not copied material from published/unpublished sources (reports, textbooks, papers, websites etc.)

3 where material from any source was used, the source was given due credit by citing it in the text of the report and giving its details in the section on references, and

4 where material from any source was copied, it was put in quotation marks, and the source was given due credit by citing it in the text of the report and giving its details in the section on references.

Signature of the author: . . . . . .

Aditya Kumar
Department of Chemical Engineering
Indian Institute of Science, Bengaluru

Acknowledgements

I would like to thank Department of Chemical Engineering for giving me an opportunity to pursue my M. Tech (Research). I am thankful to my guide Dr. S. Venugopal for providing me with his support, guidance and experimental facilities to carry out research. I am thankful for the academic freedom he provided that allowed me to explore the research area extensively. His valuable mentoring and timely intervention ensured that I steer clear from the common pitfalls in conducting research.

I would like to thank all the faculty members of the department for making course-work interesting and priming me for the research. Thanks to the all the non-teaching staff for helping with all the non-academic issues. I am thankful to the Micro and Nano Characterization facility at CeNSE for providing the access to SEM and Raman Spectrometer.

I would also like to thank my lab mates and friends, Pushkaraj, Sushant, Abhishek, Khantesh, Madhvan for their suggestions and help. I would like to thank my friends Amit, Pradyumn, Tabish, Amar, Sangram who made IISc a very great place to live in.

I would especially like to thank my friend Utkarsha who always acted as a vent for my frustrations. Finally, I would like to thank my parents and my siblings, Abhishek and Nancy for their unconditional love, encouragement, and care in all my endeavors.

Aditya Kumar

Abstract

Food adulteration is the act of degrading the quality of food by adding cheap and often toxic substances (adulterants) to profit by either improving the appearance or by improving the shelf life of the food upon storage. The use of non-permitted colours on food items is a growing menace faced by Indian consumers. For example, 'Metanil Yellow (MY)' and 'Malachite Green (MG)', carcinogenic dyes used to enhance the appearance of dals and green vegetables respectively, have been detected in ~28% of produce tested in Mysore [1]. Food Safety and Standards Authority of India (FSSAI) is the government body which sets standards and monitors the quality of food. But the process of collection of samples and preparation of samples for chemical analysis using sophisticated analytical instruments takes about 1-2 weeks to complete. This delay makes it impossible to undertake preventive action to stop the inflow of adulterated food in the market. As such, there is a definite need for a point of use chemical analysis of food adulteration in India and worldwide.

Surface Enhanced Raman Spectroscopy (SERS) is an analytical technique that is well-suited for point of use chemical analysis. A key aspect of SERS is the use of a plasmonic nanostructured substrate for amplifying the Raman signal of adsorbed molecules. Recently, our group developed a simple process for fabricating SERS-active silver nanostructures on paper [2]. This thesis discusses the application of such paper-based SERS substrates for the rapid detection of non-permitted colouring agents from pulses and vegetables by using a portable Raman Spectrometer. The concentration-based adsorption analysis showed successful detection of Rhodamine 6G, Malachite Green, and Metanil Yellow dyes in the nanomolar range. Adsorption analysis showed that Langmuir isotherm fits well in the higher concentration range but at lower concertation the model predictions were much lower than observations. This deviation at lower concentrations is attributed to the non-linear dependence of SERS intensity on adsorbed concentration due to the presence of 'hotspots'. Overall, the SERS signal variation across substrates was found to be 1.6%, which attests to the uniformity of the silver nanostructures over macroscopic areas and highlights the reproducibility of the fabrication process.

For the detection of MY in dal samples, FSSAI suggested HCl-based quick diagnostic test was found to fail when the dal samples were adulterated with MY solutions having concentration of 100 μM and lower. However, there is a significant enhancement in the appearance of dal samples adulterated with 100 μM MY solutions and thus there is an immediate need to detect MY from these samples. The SERS swabs can successfully detect MY from the dal samples adulterated even with 1 μM solution, below which there is no economic incentive to adulterate. Thus, SERS swabbing can help to detect MY adulteration in real-world dal samples. Pursuing this possibility, several real-world samples were also tested. Apart from one dal sample from a public distribution system (Ration) shop, the other samples were found to be safe. Similarly, MG dye has been successfully detected from the green peas and green chillies samples intentionally adulterated with 100 nM solution concertation of MG. Finally, to verify the claims of market-available cleaners and ozoniser, green chillies and green peas adulterated with Malachite Green were treated as prescribed and SERS results indicate that about 60-75 % of MG was removed using liquid cleaners, while ~88% removal was feasible using an ozoniser.

In conclusion, these results show the successful adaptation of SERS swabs for the rapid and portable detection of food adulteration using non-permitted colours.

[1] DownToEarth, “Rampant food adulteration in Mysore,” 2015. [Online]. Available: https://www.downtoearth.org.in/news/rampant-food-adulteration-in-mysore-4576. [Accessed: 30-Jul-2018].

[2] P. Joshi and V. Santhanam, “Paper-based SERS active substrates on demand,” RSC Adv., vol. 6, no. 72, pp. 68545–68552, 2016.

Contents

List of figures

List of tables

Chapter 1 Introduction

1.1 Motivation

Green vegetables, pulses, and spices are significant food items in the Indian diet. Lentils, beans, chickpeas and yellow peas come under the category of pulses. In the Indian diet, pulses are the primary source of micronutrients, proteins and carbohydrates with the minimum amount of fats. These pulses also provide Vitamin D, dietary fibres and many antioxidants. Adequate consumption of pulses fulfils the daily requirement of protein in Indian vegetarian diet.

Vegetables and fruits are accepted as healthy food worldwide. Green vegetables play an important role in one's diet as they are concentrated with vitamins like vitamin C, Folic acid, B complex vitamins, carotenoids (precursors of Vitamin A), phytochemicals, minerals (like iron and calcium), complex carbohydrates/fibre, and antioxidants [1]. It is suggested to have some portion of green vegetables in the meal because of its many health benefits [2]. Indian dietary guideline recommends having 100 grams of green vegetables per portion for adults [1].

It is a common belief world over that brighter the vegetables and produce appear the fresher it will be. Typically, the Indian markets have different varieties of lentils and green vegetables, and consumers tend to buy those lentils and vegetables which are bright and shiny as a dull colour is associated with bad quality, and this popular belief provides the economic incentive for illegal use of artificial colours by unscrupulous traders. Artificial colours can also be used to enhance the colour tone of the old stock of vegetables and pulses and make them look fresh. Such synthetic colourants have even been detected in packed foods and beverages [3].

Adulteration is an act of degrading the quality of food by adding cheap, inferior, and toxic substances to make produce look appealing or to improve their shelf-life for financial gain. The synthetic chemicals which are employed for this purpose are called adulterants. The continuous consumption of adulterated food results in slow poisoning and the end effect is that the consumers become the victim of illnesses caused by

adulterated food. Lack of awareness, negligence and inadequate enforcement of food laws also play a vital role in the proliferation of food adulteration.

Some of the food items in the Indian market that are reported to be adulterated include:

- Dals [4], turmeric [5], and curry powder [6], [7] that are adulterated with Metanil Yellow (MY, carcinogenic [8]) to improve the colour of the food [4]
- Green chillies, green peas (packed) and other green vegetables that are adulterated with Malachite Green (MG, carcinogenic and causes multi-organ tissue injury [9]) to make the vegetables look 'glowing' green [3]

Metanil Yellow ($C_{18}H_{15}N_3NaO_3S$) is a toxic azo dye which is banned from being used as food dye because studies have shown that Metanil Yellow under anaerobic condition, reduces to form aromatic amines posing a risk to human health [8], [10] and can lead to neurotoxicity [11], hepatocellular carcinoma [12], [13], tumour development [14], adverse effect on gastric mucin [15], and lymphocytic leukemia [16].

Malachite Green ($C_{23}H_{25}ClN_2$) is generally used as a dye in silk, leather, and paper industry. It is also used in the aquaculture industry as a fungicide [17], parasiticide, and bactericide [18] due to its carcinogenic [19], mutagenic, and teratogenic properties [8]. Malachite green has reportedly been used in green vegetables like green chillies, green peas, and leafy vegetables despite being banned worldwide.

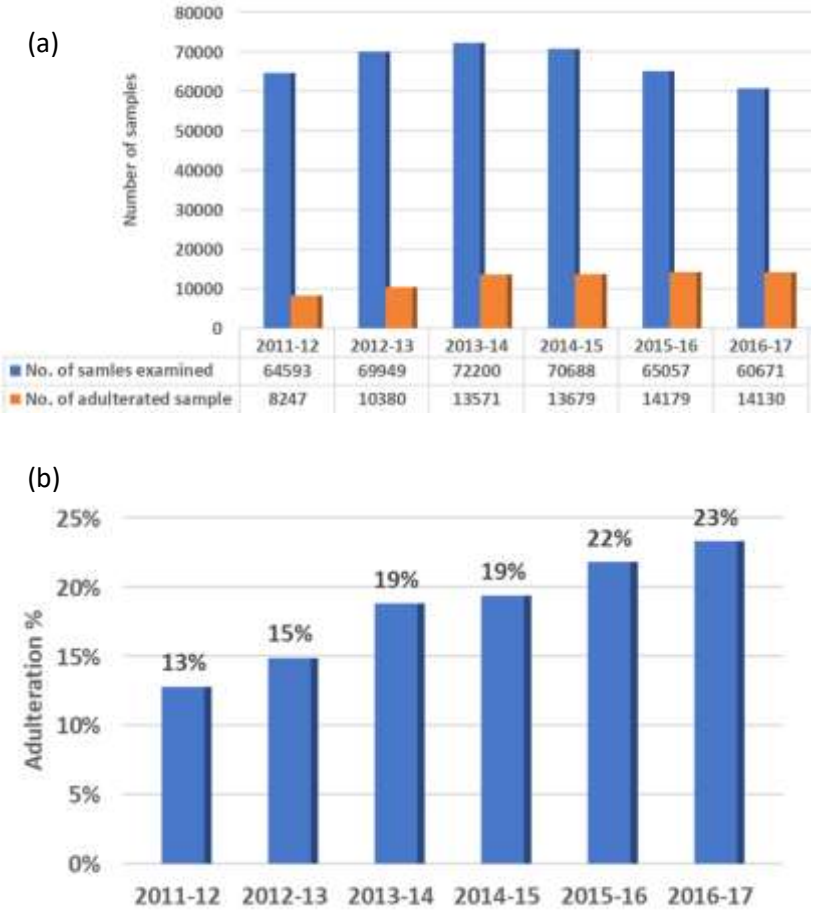

Figure 1. 1 Current food adulteration scenario in India [21].

Figure 1.1 shows the current scenario of food adulteration in India, where the extent of adulteration detected has increased from 13% to 23% in 6-7 years [20]. Food Safety and Standards Authority of India (FSSAI) is the government body which sets standards for articles of food and regulates their manufacturing, storage, distribution, sale and import to ensure availability of safe and wholesome food for human consumption in India. FSSAI ensures the quality of food by testing them in their laboratories. The conventional chemical analytical methods employed for the detection of food adulteration involve three steps, a collection of samples from the market and transporting the samples to the laboratories, a sample preparation step and then detection with either Gas chromatography-Mass spectroscopy (GC-MS) or Liquid chromatography-Mass spectroscopy (LC-MS), or High-pressure liquid

chromatography (HPLC). As shown in Figure 1.2, the sample preparation step involves grinding and blending of food item followed by extraction of target organic molecules into the organic phase for further analysis using chromatographic techniques. But, the entire process from collection of samples to analysis takes about 1-2 weeks to complete, while a national report on the statistics of adulterants detected is published annually. These delays make it impossible to undertake preventive action to stop the inflow of adulterated food into the market. Hence, there is a definite need for low-cost technologies that can enable point of use adulterant detection.

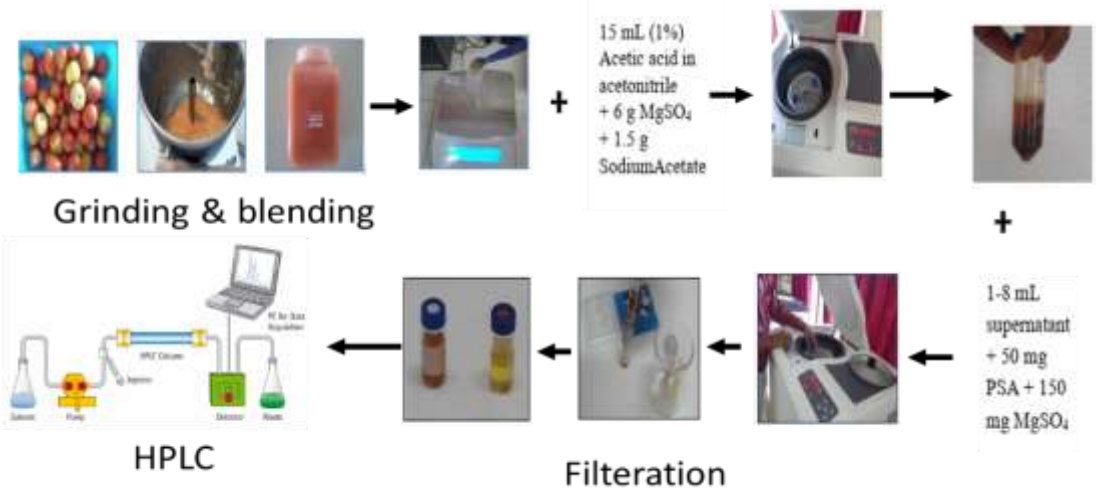

Figure 1. 2 conventional sample preparation method for detecting adulterants in food samples

Nanomaterials are promising materials for fabricating sensors due to their tunable optical properties [21], physicochemical properties [22], and catalytic activity [23]., Surface Enhanced Raman Spectroscopy (SERS) is a capable technique for rapid, on-field detection of Raman spectra of molecules. The vibrational signature encoded in the Raman spectra can be used as a unique identifier of molecular structure. A plasmonic nanostructured substrate is required for amplification, by several orders of magnitude, of the weak Raman signal (almost exclusively emitted from the adsorbed molecular layer closest to the surface), and such 'surface-enhancement' renders SERS capable of detecting the presence of a single molecule [24].

Silver-based nanostructures have optimal plasmonic properties giving rise to higher SERS enhancement factors as compared to other materials [23]. However, commercially available silver SERS substrates (Silemco [23], Q-SERS [23], and Diagnostic anSERS [25]) have a limited shelf life of ~3-6 weeks since the activity of silver substrate decreases with time due to tarnishing under environmental conditions. So, for improving shelf-life up to 12-24 weeks, these substrates are packaged and stored under inert condition [25], which considerably increases their cost. Thus, it is quite a challenge to fabricate low-cost disposable silver SERS substrates for on-field application.

1.2 Aim and structure of Thesis

Recently, a simple desktop printer based low-cost fabrication of paper-based SERS-active silver nanostructures was reported by our group [26, 27]. The process obviates the need for storage under inert conditions as substrates can be fabricated on demand. The goal of this research was to develop optimal protocols for the use of paper-based SERS substrates for onsite detection of adulterants from food items. The specific objectives were the detection of synthetic colourants used in the adulteration of pulses, and green vegetables using a portable Raman Spectrometer.

This thesis reports results on the detection of two commonly used adulterants, namely ‘Metanil Yellow (MY)’ from the surface of pulses, and ‘Malachite Green (MG)’ from the skin of vegetables using a portable Raman Spectrometer from Snowy Range Instruments (SnRI) [29]. Chapter 1 provides an overview of the current scenario of food adulteration in India, the drawbacks associated with existing detection techniques, and the proposed solution based on paper-based SERS substrates. Chapter 2 reviews the basic concepts useful for understanding Raman scattering and surface enhancement of the Raman signal. Chapter 3 provides information about the inkjet printing method used for the fabrication of SERS substrate and a review of selected literature reports on SERS. Chapter 4 covers the experimental part which involves the optimization of the acquisition condition for spectra in portable Raman Spectrometer and then presents results on the detection of adulterants from food samples. Finally, chapter 5 summarises

and lists the conclusions based on our analysis of the results and ends with a discussion on the scope for future work.

REFERENCES

[1] R.T. Kamala K, Bhaskaram P, Bhat RV, Dietary Guidelines for Indians- A Manual, Natlional Institute of Nutrition, 3 (2011), http://ninindia.org/DietaryGuidelinesforNINwebsite.pdf (accessed June 24, 2018).

[2] J. L. Slavin and B. Lloyd, "Health Benefits of Fruits and Vegetables," *Adv. Nutr.*, vol. 3, no. 4, pp. 506–516, Jul. 2012.

[3] V. Ashok, N. Agrawal, A. Durgbanshi, J. Esteve-Romero, and D. Bose, "Determination of Adulteration of Malachite Green in Green Pea and Some Prepared Foodstuffs by Micellar Liquid Chromatography," *J. AOAC Int.*, vol. 97, no. 5, pp. 1387–1392, Sep. 2014.

[4] B. V Sudheer, M. K. Lakshmidevi, and D. V Krishna Rao, "Adulteration of the pulses in coastal region of Andhra Pradesh," *J Evol. Med Dent Sci J. Evol. Med. Dent. Sci.*, vol. 4, no. 36, pp. 6187–6192, 2015.

[5] S. Dhakal, K. Chao, W. Schmidt, J. Qin, M. Kim, and D. Chan, "Evaluation of Turmeric Powder Adulterated with Metanil Yellow Using FT-Raman and FT-IR Spectroscopy," *Foods*, vol. 5, no. 2, p. 36, 2016.

[6] S. Dhakal, K. Chao, W. Schmidt, J. Qin, M. Kim, and Q. Huang, "Detection of Azo Dyes in Curry Powder Using a 1064-nm Dispersive Point-Scan Raman System," *Appl. Sci.*, vol. 8, no. 4, p. 564, Apr. 2018.

[7] S. Dhakal, K. Chao, M. S. Kim, J. Qin, and A. Bae, "Detection of color dye contamination in spice powder using 1064 nm Raman chemical imaging system," in *Sensing for Agriculture and Food Quality and Safety X*, 2018, vol. 10665, p. 7.

[8] E. Sudova, J. Machova, Z. Svobodova, and T. Vesely, "Negative effects of malachite green and possibilities of its replacement in the treatment of fish eggs and fish: A review," *Vet. Med. (Praha).*, vol. 52, no. 12, pp. 527–539, 2007.

[9] S. Srivastava, R. Sinha, and D. Roy, "Toxicological effects of malachite green," *Aquat.*

Toxicol., vol. 66, no. 3, pp. 319–329, Feb. 2004.

[10] P. Vineis and R. Pirastu, “Aromatic amines and cancer,” *Cancer Causes Control*, vol. 8, no. 3, pp. 346–355, 1997.

[11] T. N. Nagaraja and T. Desiraju, “Effects of chronic consumption of metanil yellow by developing and adult rats on brain regional levels of noradrenaline, dopamine and serotonin, on acetylcholine esterase activity and on operant conditioning.,” *Food Chem. Toxicol.*, vol. 31, no. 1, pp. 41–4, Jan. 1993.

[12] B. Saxena and S. Sharma, “Food Color Induced Hepatotoxicity in Swiss Albino Rats, Rattus norvegicus.,” *Toxicol. Int.*, vol. 22, no. 1, pp. 152–7, 2015.

[13] C. Fernandes and K. V Rao, “Dose related promoter effect of metanil yellow on the development of hepatic pre-neoplastic lesions induced by N-nitrosodiethylamine in rats.,” *Indian J. Med. Res.*, vol. 100, pp. 140–9, Sep. 1994.

[14] S. Gupta, M. Sundarrajan, and K. V. K. Rao, “Tumor promotion by metanil yellow and malachite green during rat hepatocarcinogenesis is associated with dysregulated expression of cell cycle regulatory proteins,” *Teratog. Carcinog. Mutagen.*, vol. 23, no. S1, pp. 301–312, 2003.

[15] H. Raza, S. K. Khanna, and G. B. Singh, “Metanil yellow & gastric mucin.,” *Indian J. Exp. Biol.*, vol. 16, no. 3, pp. 383–4, Mar. 1978.

[16] O. M. Prasad and P. B. Rastogi, “Haematological changes induced by feeding a common food colour, metanil yellow, in albino mice,” *Toxicol. Lett.*, vol. 16, no. 1–2, pp. 103–107, Apr. 1983.

[17] C. J. Cha, D. R. Doerge, and C. E. Cerniglia, “Biotransformation of malachite green by the fungus Cunninghamella elegans.,” *Appl. Environ. Microbiol.*, vol. 67, no. 9, pp. 4358–60, Sep. 2001.

[18] J. M. van de Riet, C. J. Murphy, J. N. Pearce, R. A. Potter, and B. G. Burns, “Determination of malachite green and leucomalachite green in a variety of aquacultured products by liquid chromatography with tandem mass spectrometry detection.,” *J. AOAC Int.*, vol. 88, no. 3, pp. 744–9.

[19] C. Fernandes, V. S. Lalitha, and K. V Rao, “Enhancing effect of malachite green on the development of hepatic pre-neoplastic lesions induced by N-nitrosodiethylamine in

rats.," *Carcinogenesis*, vol. 12, no. 5, pp. 839–45, May 1991.

[20] FSSAI Annual Reports 2011-17, Ministry of Health and Faminly Welfare (2017). https://www.fssai.gov.in/home/FSSAI-Annual-Reports.html (accessed October 26, 2018).

[21] J. J. Mock, M. Barbic, D. R. Smith, D. A. Schultz, and S. Schultz, "Shape effects in plasmon resonance of individual colloidal silver nanoparticles," *J. Chem. Phys.*, vol. 116, no. 15, pp. 6755–6759, Apr. 2002.

[22] Q. Jiang, S. Zhang, and M. Zhao, "Size-dependent melting point of noble metals," *Mater. Chem. Phys.*, vol. 82, no. 1, pp. 225–227, Sep. 2003.

[23] R. N. and M. A. El-Sayed, "Shape-Dependent Catalytic Activity of Platinum Nanoparticles in Colloidal Solution," 2004.

[24] K. Kneipp *et al.*, "Single Molecule Detection Using Surface-Enhanced Raman Scattering (SERS)," *Phys. Rev. Lett.*, vol. 78, no. 9, pp. 1667–1670, Mar. 1997.

[25] W. Sers, "P - SERS Technology Technical Paper P-SERS— Trace detection overcoming the cost and usability limitations of traditional SERS technology," pp. 1–8, 2015.

[26] S. K. Parmar and V. Santhanam, "In situ formation of silver nanowire networks on paper," *Current Science*, vol. 107. Current Science Association, pp. 262–269.

[27] P. Joshi and V. Santhanam, "Paper-based SERS active substrates on demand," *RSC Adv.*, vol. 6, no. 72, pp. 68545–68552, Jul. 2016.

[28] "Sierra - SnRI." [Online]. Available: http://www.wysri.com/sierra/. [Accessed: 25-Jun-2018].

Chapter 2 Raman Spectroscopy and SERS

4.1 Introduction

Spectroscopy is the study of the interaction between electromagnetic waves and matter; incident electromagnetic radiation is either absorbed or scattered by matter. Raman Spectroscopy is concerned with the scattered radiation from a sample. Scattering refers to a change in the direction of light as it propagates through a medium. Scattering can be envisioned as the simultaneous absorption of incident photon and emission of another photon (scattered photon) in a different direction.

Depending upon the energy of the scattered photon with respect to the incident photon, scattering can be classified into 1) Elastic scattering, and 2) Inelastic scattering. A scattering event is termed elastic when the energy of the scattered photon, E_S, is equal to that of the incident photon, $E_{L;}$ wherein molecules within the matter return to the same energy level after the scattering, as illustrated in Figure 2.1 (a). Elastic scattering is also referred to as Rayleigh Scattering. On the other hand, a scattering event is called inelastic when the energy of the scattered photon, E_S, is different from that of the incident photon, E_L. The energy difference, E_S - E_L, corresponds to the energy difference required for transition between any two molecular states, as illustrated in Figure 2.1 (b). Raman Scattering is a form of inelastic scattering, where the shift in the energy of the scattered photon with respect to the incident one corresponds to transition between the vibrational/rotational levels.

In principle, after absorption of a photon, the molecule should be excited to a higher energy level. In the case of Raman scattering, this higher energy level may not be one of the stationary states of the molecule. In that case, transition probabilities for Raman scattering can be best understood as being computationally equivalent to a superposition of the electronic wavefunctions associated with the '*virtual state'* and the initial or final states corresponding to absorption or emission, which are taken as

'simultaneous and instantaneous'. The virtual state has no physical significance, in general, and is just a mathematical representation of the higher energy level in quantum perturbation theory. Figure 2.2 illustrates the process of Rayleigh and Raman scattering through the quantum mechanics point of view. If virtual state coincides with a real electronic level (say any vibronic level in S_1), then such kind of scattering is called resonant scattering.

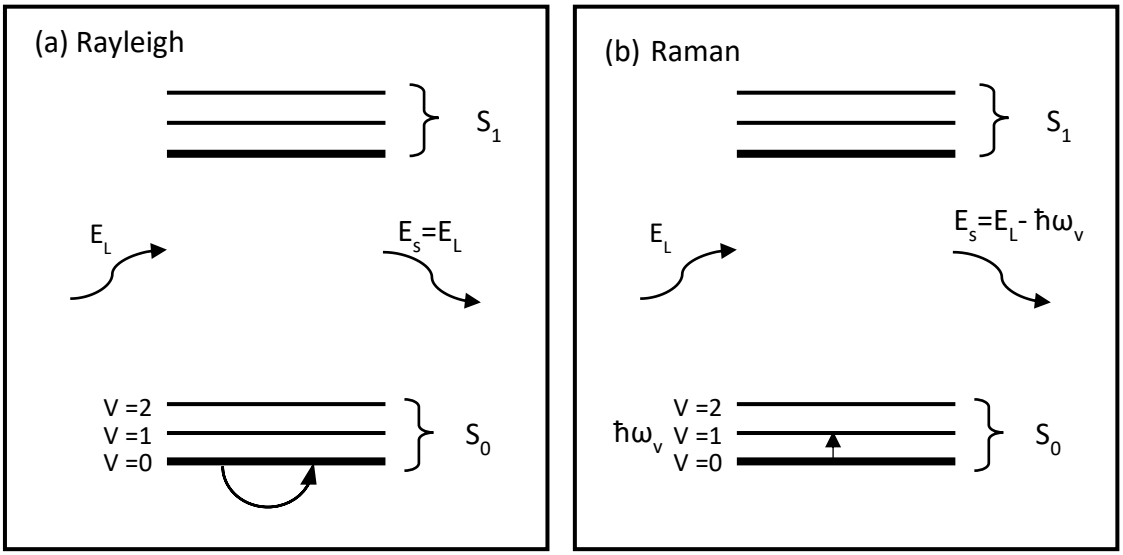

Figure 2.1 Jablonski diagrams schematically illustrating (a) Rayleigh and (b) Raman Scattering. S_0 and S_1 are primary electronic levels and v=0, 1, 2 are the sub-electronic (vibronic) levels. In Rayleigh scattering molecule comes back to the same energy level, v=0, after scattering, while in Raman scattering the molecule has returned to a different energy level (from v = 0 to v = 1) after scattering, and a photon is scattered with the energy E_S wherein $\hbar\omega_V$ is the energy required for the transition. Reproduced from Eric C. Le Ru and Pablo G. Etchegoin [1].

Raman scattering can be further divided into two parts Stokes and Anti-Stokes process depending upon the Raman shift, defined as the difference in the energy of the incident and scattered photon.

$$\Delta E = E_L - E_S \tag{2.1}$$

In Stokes process, the energy of the scattered photon is less than that of the incident one ($E_S < E_L$) which results in the excitation of the molecule from the vibrational ground level v= 0 to the first vibrational excitation state v = 1 as shown in Figure 2.3 (a).

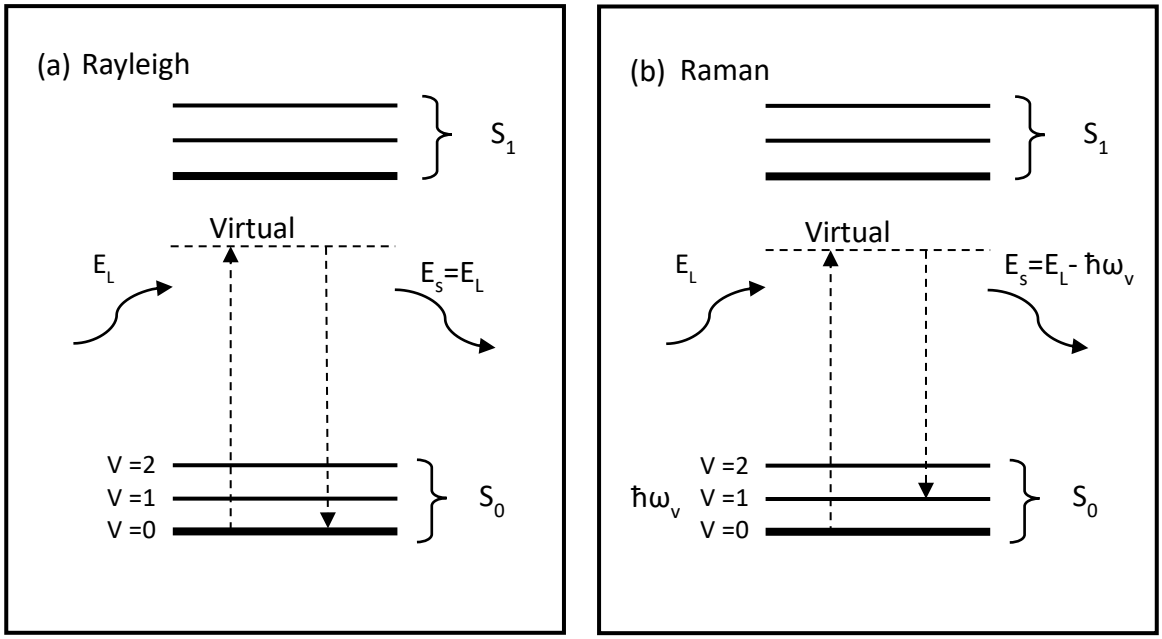

Figure 2.2 Jablonski diagrams schematically illustrating (a) Rayleigh and (b) Raman Scattering through quantum mechanics point of view. The absorption of the photon is through a transition of a molecule to a virtual state, and a photon is scattered when molecule comes back to same vibronic level (a), or to a different vibronic level (b). The virtual state may or may not coincide with a stationary electronic state of the molecule, in case if it coincides then it is called resonant. Reproduced from Eric C. Le Ru and Pablo G. Etchegoin [1].

In the anti-Stokes process, the energy of the scattered photon is more than that of the incident photon's energy ($E_S > E_L$). As illustrated in Figure 2.3 (b) molecule transitions from the excited vibrational level v = 1 to ground vibrational level v = 0. For this process to occur, the molecule should initially be in the excited vibrational level, which is typically less populated than the ground level. As a result, Raman signal intensity is very weak in anti-Stokes Raman process compared to Stokes Raman process.

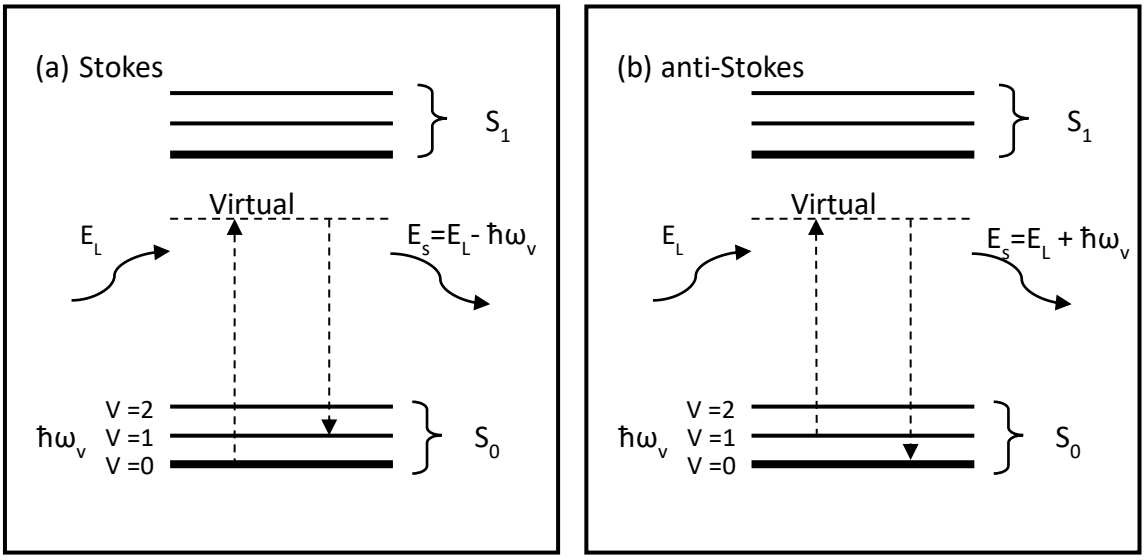

Figure 2.3 Jablonski diagrams of the (a) Stokes and (b) anti-stokes Raman process. Reproduced from Eric C. Le Ru and Pablo G. Etchegoin [1].

The origin of Raman effect can be understood in the classical electromagnetic field description using the concept of *polarizability* of a molecule. Polarizability refers to the phenomenon that when the electric field of an electromagnetic wave (Light) is incident upon a molecule, negatively charged electrons and positively charged nuclei are attracted towards the positive and negative pole of the incident field respectively. This results in the 'polarization' of a molecule, and it creates an induced electric dipole moment in the molecule. These dipole moments are typically mapped onto specific atomic bonds within the molecules. Interaction of incident electromagnetic light with these induced dipoles can lead to energy transfer that results in altering the vibrational or rotational energy levels of these bonds. A key insight is that molecular transition between modes of vibrations that result in a change in polarizability give rise to the corresponding peaks in Raman spectroscopy. Thus, a Raman spectrum is a 'molecular' signature containing information on the bonds present within a molecule. From a technological standpoint, the Raman spectral signature region is not obscured by the presence of water vapour, and thus, it is unaffected by humidity, which opens avenues for on-field deployment.

4.2 Role of metals in enhancing Raman signal

Metals such as silver (Ag), gold (Au), copper (Cu), or aluminium (Al) are known to have excellent thermal and electrical conductivity due to the presence of a 'sea' of free conduction electrons that move around in a background of the positive ions ensuring the overall charge neutrality. The collective behaviour of these free conduction electrons is modelled as a single entity and denoted as a *plasma* (free electron plasma or solid-state plasma) and *plasmons* denote the corresponding quantum of plasma oscillations. The optical response of the free electron plasma can be understood by the Drude-Lorentz model, which describes the dependence of dielectric constant on the frequency ω of the electromagnetic field. The optical response can be well understood by the following complex dielectric constant of metal, ε_{in} [1].

$$\varepsilon_{in} = \epsilon_{\infty}\left(1 - \frac{\omega_p^2}{\omega^2 + i\gamma_0\omega}\right) \tag{2.2}$$

Where ω_p is the natural oscillation frequency of the free electron plasma, also called as plasma frequency, and is defined as

$$\omega_p = \sqrt{\frac{ne^2}{m\epsilon_0\epsilon_{\infty}}} \tag{2.3}$$

Real and imaginary parts of the complex dielectric function are given as follows

$$R_e(\varepsilon_{in}) = \epsilon_{\infty}\left(1 - \frac{\omega_p^2}{\omega^2 + \gamma_0^2}\right) \tag{2.4}$$

$$Im(\varepsilon_{in}) = \frac{\epsilon_{\infty}\omega_p^2\gamma_0}{\omega(\omega^2 + \gamma_0^2)} \tag{2.5}$$

Where n is the number of free electrons per unit volume and m is their mass. γ_0 is the damping term, which corresponds to the collision rate of the free electron with the crystal, ϵ_∞ is the background dielectric function, ϵ_0 is vacuum electric permittivity.

The negative value of the real part of ϵ, is the origin of many optical properties of metals in the visible and IR range, as it is related to the existence of plasmons and its response. The imaginary part is related to the range of the collective response. The effect of an incident electromagnetic field on the dynamics of the plasmon within a nanostructure can be well understood using the quasistatic approach, i.e. considering a *small metallic sphere (radius a) much smaller than the wavelength of the incident electromagnetic field wavelength(λ) (*a << λ limit leads to the uniform static electric field around the nanoparticle (Figure 2.4)*)*. This problem then reduces to the problem of the response of a metallic sphere (dielectric constant ϵ_{in}), embedded in a medium of relative dielectric constant ϵ_{out}, to an external electric field, $\mathbf{E}_0$. Under the condition of the uniform electric field around the metallic particle Maxwell's equation can be solved by approximating it to Laplace's equation to determine the field inside (E_{In}) [2] and outside (at the surface, E_{out}) of the sphere [3]

$$E_{In} = \left(\frac{3\epsilon_{out}}{\epsilon_{in} + 2\epsilon_{out}}\right) E_0 \tag{2.6}$$

$$E_{out} = E_0\boldsymbol{z} - \alpha E_0\left(\frac{\boldsymbol{z}}{r^3} - \frac{3\boldsymbol{z}}{r^5}(z\boldsymbol{z} + x\boldsymbol{x} + y\boldsymbol{y})\right) \tag{2.7}$$

$$\alpha = ga^3 \tag{2.8}$$

and

$$g = \frac{\epsilon_{in} - \epsilon_{out}}{\epsilon_{in} + 2\epsilon_{out}} \tag{2.9}$$

Where the first term, $E_0\boldsymbol{z}$, is the applied field, and second term, $\alpha E_0(\ldots)$, is the induced dipole which results from the polarization, due to the applied electric field, of the electron density in the metal sphere. α is the metal polarizability, $x, y, z, \boldsymbol{x}, \boldsymbol{y}, \boldsymbol{z}$ are the normal cartesian coordinates and unit vectors, respectively, r is the radial distance, E_0 is the magnitude of $\mathbf{E}_0$, and E_{out} is the electric field at the surface of the sphere ($r = a$).

The electric field 'outside' the metal sphere can be enhanced for a significant value of g. This can be achieved when the denominator of g tends to zero, which implies $\epsilon_{in} \approx -2\epsilon_M$. For standard dielectrics, ϵ is in between 1 to 10, so a large electric field is not possible. But in the case of metals, it is possible to achieve at the wavelength for which absorption is small ($Im(\epsilon_{in}) \approx 0$), and $Re(\epsilon_{in}) \approx -2\epsilon_M$. In the visible and IR range, $\omega < \omega_p$, $Re(\epsilon_{in})$ becomes negative. The large change in the optical response (internal electric field) of plasmons gives rise to *resonance*. Resonance occurring at $Re(\epsilon_{in}) \approx -2$ (for metal nanoparticles in air ($\epsilon_M = 1$)), is referred to as *localized surface plasmon resonance (LSPR)*. LSPR of metallic nanoparticles under the influence of external electromagnetic field is schematically illustrated in Figure 2.4.

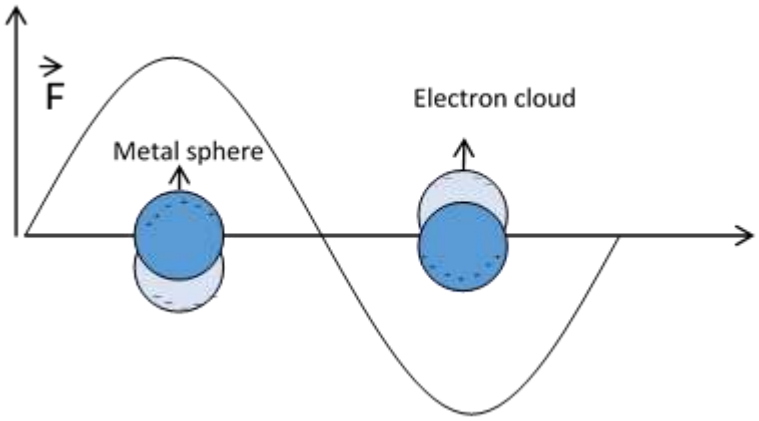

Figure 2.4 Illustration of LSPR of metal nanoparticle under the influence of external electromagnetic field.

Resonance conditions in the small metallic object are strongly related to the geometry of the object. Two metallic objects with different geometries will have different resonance response. The resonance conditions are also dependent on the optical absorption, where optical absorption is expressed by the imaginary part of ϵ_{in} (larger

the $Im(\epsilon_{in})$, the resonance will be weaker). Strength (width) of the resonance is characterized by the *quality factor*, denoted by Q,

$$Q = \frac{\omega\left(\frac{d\ Re(\epsilon_{in})}{d\omega}\right)}{2(Im(\epsilon_{in}))^2} \tag{2.10}$$

The quality factor will be substantial for a small value of $Im(\epsilon_{in})$, which results in a larger electric field intensity on the surface at resonance.

4.3 Surface Enhanced Raman Spectroscopy (SERS)

SERS was first reported in 1977 when a study showed the Raman signal intensity of a scatterer (pyridine) could be increased by a significant factor when the scatterer is adsorbed on an electrochemically roughened nanostructured silver surface [4]. The enhancement of the electric field near the surface of the metallic nanostructure leads to significant enhancement of the Raman signal of the molecules adsorbed on the metal surface. The use of this phenomenon to acquire Raman spectra is denoted as SERS.

With $Re(\epsilon_{in}) \approx -2$ in visible and IR range, metals are excellent candidates for SERS, but metals like aluminium, platinum, and palladium are ruled out because they have a low quality-factor as compared to silver, gold and copper. Amongst these, silver is most suitable for practical application (widely used for SERS) since gold and copper have a lower quality factor in most part of the visible spectrum, and they are only suitable for excitation in the near IR region. Furthermore, the resonance condition in the metal can also be tuned by changing the geometry (size and shape). Metal nanoparticles, nanowires, core-shell alloy etc. are generally employed for the plasmonic application (especially in SERS).

In SERS, if we consider a molecule positioned near the surface at the maximum enhancement ($|g| >> 1$), both the incident and scattered photons experience the intense electric field leading to an overall enhancement factor that is approximated as

$$EF = \frac{|E_{out}|^2 |E'_{out}|^2}{|E_0|^2} = 16|g|^2|g'|^2 \quad (2.11)$$

Here E'_{out} and g' are evaluated at the scattered frequency, and EF is the SERS enhancement factor.

For small Stokes shifts, $|g|$ and $|g'|$ are approximately the same and EF scales as $|g|^4$, which is known as the E^4 enhancement or electromagnetic enhancement. Thus, if the electric field enhancement at the plasmonic surface is 10x, the overall enhancement in the molecule SERS intensity will be 10^4 times.

4.4 Distance dependence of EF

As discussed earlier, enhancement of Raman signal depends upon the type of metal, size, and shape of the metallic nanostructure. The field enhancement around the metal sphere depends upon the radii of curvature of the plasmonic feature, a, and the distance from the feature, r [5]. The field enhancement around the sphere decays with r^{-3}, and in the case of E^4 enhancement, the enhancement decays as r^{-12}. In the case of SERS, the surface area is increased by the scale of r^2 in comparison to a flat surface due to the presence of scattered molecule near (or on) the metal nanoparticle, which finally leads to r^{-10} distance dependence of EF. The decrease in the Raman mode intensity is given by

$$I_{SERS} = \left(1 + \frac{r}{a}\right)^{-10} \quad (2.13)$$

Where I is the intensity of Raman mode, a is the average size of the field enhancing roughness feature on the metal surface, and r is the distance from the surface to adsorbate [6].

REFERENCES

[1] E.C. Le Ru, P.G. Etchegoin, Chapter 2 - Raman spectroscopy and related optical techniques, in: E.C. Le Ru, P.G. Etchegoin (Eds.), Princ. Surface-Enhanced Raman Spectrosc., Elsevier, Amsterdam, 2009: pp. 29–120. doi:https://doi.org/10.1016/B978-0-444-52779-0.00008-8.

[2] J.D. Jackson, Classical Electrodynamics, 3rd ed., Am. J. Phys. 67 (1999) 841. doi:10.1119/1.19136.

[3] G.C. Schatz, R.P. Van Duyne, J.M. Chalmers, P.R. Griffiths, Electromagnetic Mechanism of Surface-enhanced Spectroscopy Handbook of Vibrational Spectroscopy Surface-enhanced Vibrational Spectroscopy Electromagnetic Mechanism of Surface-enhanced Spectroscopy, (n.d.). https://cpb-us e1.wpmucdn.com/sites.northwestern.edu dist/f/44/files/2012/10/2002_Schatz.pdf (accessed July 6, 2018).

[4] D.L. Jeanmaire, R.P. Van Duyne, Surface raman spectroelectrochemistry: Part I. Heterocyclic, aromatic, and aliphatic amines adsorbed on the anodized silver electrode, J. Electroanal. Chem. Interfacial Electrochem. 84 (1977) 1–20. doi:10.1016/S0022-0728(77)80224-6.

[5] P.F. Liao, A. Wokaun, Lightning rod effect in surface enhanced Raman scattering, J. Chem. Phys. 76 (1982) 751–752. doi:10.1063/1.442690.

[6] B. J. Kennedy, S. Spaeth, and M. Dickey, K.T. Carron, Determination of the Distance Dependence and Experimental Effects for Modified SERS Substrates Based on Self-Assembled Monolayers Formed Using Alkanethiols, (1999). doi:10.1021/JP984454I.

Chapter 3 Fabrication of SERS substrate and performance characterization

3.1 Literature review

Surface Enhanced Raman Spectroscopy was first observed in 1974 while studying the adsorption of pyridine at a silver electrode with high surface area [1]. Then in 1977, another group verified the earlier result and confirmed the enhancement in the Raman scattering of molecules adsorbed onto a 'rough' surface. This enhancement in the Raman signal due to the roughened surface was denoted as Surface Enhancement Raman Spectroscopy (SERS) [2]. Over the years SERS has significantly benefitted from advances in the area of nanostructured materials. Even single molecule detection was achieved using SERS [3].

The potential for application of SERS ranges from biochemistry and bio-sensing, polymer and material science, to catalysis, and electrochemistry. Being a highly sensitive and selective molecular detection technique, SERS based sensors are found to be useful in the detection of adulterants [4]–[6], pesticides [7], explosives [8]–[10], environmental pollutants [11], nuclear waste [12], drugs [11], biomolecules [13]–[17], bacteria [16], and fingerprints [17].

Given the crucial role of metallic nanostructures, significant research effort has also been focused on the low-cost fabrication of highly sensitive, uniform, and reproducible nanostructured substrates [18]. The first ever SERS substrate used was fabricated using electrochemical oxidation-reduction cycles to get roughened surface [2]. The disadvantage of this method is that there is no control on the morphology of the substrate, which leads to a spatially non-uniform SERS signal [19].

Flexible SERS substrate on cellulose paper was initially prepared by thermal evaporation of metal [22 - 24]. Recently, flexible metal sponges with a higher surface area have been generated by etching with acid. These sponges have better SERS enhancements and thermal stability as compared to a substrate fabricated by thermal evaporation [21]. Bimetallic (Au-Pt-Au) nanorods were fabricated by electrochemical deposition of metal inside a porous membrane for SERS application [22]. Another fabrication approach involves the use of a colloidal solution of metal nanoparticles. The possibility of formation of SERS enhancement '*hotspots*' in a colloidal solution of metal nanoparticles is high due to nanoparticle flocculation, and it is beneficial if the molecule is sandwiched within such a hotspot [23]. Morphology of SERS active nanostructure also affects the enhancement factor, and several groups have synthesized silver nanospheres, nanorods, and triangular nano-prisms to improve SERS performance [24], [25].

A novel method using anisotropic etching was recently reported with the ability to modify and control the morphology chemically [26]. To understand the relationship between nanoparticle structure and activity, optical and structural properties of dimers to heptamers of gold nanoparticles on a SiO_2 substrate were systematically investigated and the study showed no significant change in the enhancement factor. The average EF was found to be 1.0×10^8, with individual values ranging from 6.6×10^6 to 4.8×10^8 [27]. Although colloidal solutions can provide high SERS enhancements, their synthesis involves cumbersome and tedious liquid-handling protocols that are not suited for on-site detection of adulterants.

For rapid detection of adulterants in the field using disposable SERS substrates, simple processes that result in low-cost SERS substrates are required. Therefore, fabrication processes that involve the use of photolithography, thermal evaporation, or other physical deposition processes requiring vacuum equipment are ruled out. A promising recent development involves the use of commercially available inkjet printers or liquid filtration techniques for depositing colloidal nanoparticles to form paper-based SERS substrates. These include reports on adsorption from pre-prepared colloidal solution [32-34], brushing [30], seeded growth [31], self-assembly [32], screen printing [33], and inkjet printing [34], [35]. Our group has taken a further step in the direction of

frugal engineering of disposable SERS substrates by adapting well-established technology of silver halide photographic processing to form silver nanostructures on paper substrates using print-expose-develop steps; thereby, eliminating the need for pre-synthesizing stable colloidal formulations [36], [37] [7], [38]. Moreover, the fabrication using office inkjet printer does not require any specific skill set, and it can be performed easily around the world.

A schematic summary of the steps involved in the print-expose-develop process is shown in Figure 3.1. Briefly, the steps are as follows:

1) Printing of potassium halide (KX) salt solution followed by silver salt solution ($AgNO_3$) to form silver halide film on the desired substrate,
2) The film after printing is exposed to halogen lamp which forms latent silver clusters within silver halide film,
3) Then the film is dipped into the developing solution to form silver nanowires on the desired substrate followed by rinsing with DI water to remove the residue of the developer solution.

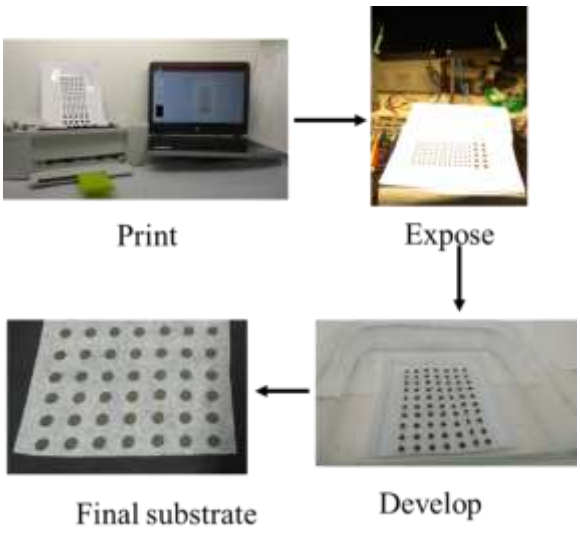

Figure 3.1 Schematic representation of the steps in print-expose-develop process

Moreover, the development step can be performed just prior to use, and this avoids issues related to lowering of SERS enhancements upon storage in ambient conditions, due to the tarnishing of silver. Thus, there is no need for special packaging of these substrates, which further eliminates costs associated with inert gas packaging of commercially available paper-based substrates.

3.2 Experimental protocol used for fabrication of SERS substrates

The first step in the fabrication of SERS substrate is to prepare a solution of salts ($AgNO_3$ & KX) in DI water (MilliQ system,18.2 MΩ.cm resistance @ 26.3 C). Note: tap water can also be used, but all the results reported in this work use DI water to avoid any chance of confusion regarding chemical compositions. Before the preparation of salt solutions, the beakers were cleaned thoroughly with DI water to avoid any contamination. The molar ratio of $AgNO_3$: KX was maintained as 1:2 for complete conversion of silver nitrate to silver halide. Potassium halide (KX) used in this work is a mixture of potassium bromide (KBr) and potassium iodide (KI) in the ratio of 95:5 by weight. Iodide being added to improve the photosensitivity of the resulting silver halide film to visible light and to form nanowires [39]. $AgNO_3$ & KX solutions were sonicated (Branson 2510 ultrasonic cleaner) for 15 mins to ensure dissolution of the salts and to form a uniform and transparent solution. Then both the solutions were filtered using a syringe filter (MILLEX GV filter unit 0.22 µm) to remove any dirt from silver nitrate and potassium halide solution. This step is a precaution to avoid clogging of the inkjet printheads. After the filtration, the $AgNO_3$ solution is stored in the dark to avoid reduction of the silver solution under ambient conditions. The concentrations of $AgNO_3$ and KX solutions used were 1 mM and 2 mM respectively.

HP (Hewlett-Packard) Deskjet 1010 inkjet printer with HP 802 ink cartridge was used for the printing of silver and potassium salts. Separate cartridges for each solution was used to avoid any chance of aqueous metathesis reaction occurring within the cartridges. For use in salt printing, a new ink cartridge was prised open, and the sponge containing the ink was removed. Then the cartridge was cleaned thoroughly with tap water followed by DI water to wash out the ink. Then the cartridge was sonicated for

20 mins, and DI water was printed a few times to ensure that no ink was left in the cartridge. Printing of known shapes using DI water solutions was used to estimate the average amount of solution printed per unit footprint area of the paper substrate (amount of silver per cm^2). The average of the volume per print of water was estimated from a decrease in the weight of the cartridge after printing ten times. On average, the print volume in each print was found to be in the range of 1.2 – 1.6 $\mu L/cm^2$. Based on this value, the nominal value of 1 mg/cm^2 of silver loading was achieved by the printing of 1 mM silver nitrate solution six times.

The silver halide film was formed on Kimwipe tissue paper by printing potassium and silver salt solutions from separate cartridge alternatively for 6 cycles each. After each print cycle, the substrate was allowed to dry to minimize photoreduction of silver nitrate (If not appropriately followed, the substrate becomes dark due to photoreduction of silver nitrate). On printing KX and $AgNO_3$, green silver halide film is formed. Once the required number of the print cycles are done, the substrate with silver halide film is exposed to a halogen lamp (500 W, Crompton Greaves Ltd) for 15 min at a distance of 50 cm to avoid overheating of the paper substrate. This step results in the formation of the latent silver clusters (3–4 atom clusters) by the photoreduction of silver halide. After the exposure step, the substrate is developed using chemical developer solution, D-76 (photographic developer) [40]. A typical composition of the developer solution is listed in Table 3.1. The substrate is kept in the developer solution for 15 mins to reduce the silver salt into silver completely. The developer solution contains reducing agents (Metol and quinone), which donate electrons to the silver ions with the ‘latent silver clusters’ acting as catalysts. After development, SERS substrate is rinsed thoroughly with DI water to remove developer solution residue. The benefit of SERS substrate fabrication by the print-expose-develop technique is that the substrate after exposing to halogen lamp can be stored for extended period of time (>52 weeks) and can be developed at the time of application.

Table 3.1 Composition of Developer solution D76

Chemical	**Quantity (for 100 mL solution in DI water)**
Metol	266.67 mg
Sodium Sulphite anhydrous	13.33 gm
Hydroquinone	666.67 mg
Borax salt	266.67 mg

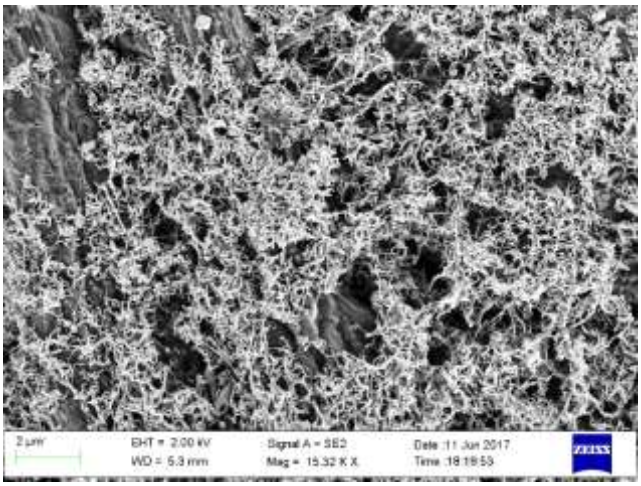

Figure 3.2 Representative FESEM image of developed silver nanowires with a nominal silver loading of 1 mg/cm^2 on Kimwipe tissue paper.

3.3 Raman spectrometer

SERS analysis was performed using a portable Raman Spectrometer (6 lb), Sierra 532 from Snowy Range Instrument (SnRI, Metrohm Raman) equipped with 532 nm laser and thermoelectric (TE) cooled 2048-pixel CCD detector. The maximum laser power is 50 mW, and incident power can be adjusted from 0 to 50 mW with the step size of 0.33 mW. Spectra acquisition is controlled by the “Peak” software. The Raman Spectrometer comes with ‘Three-way sampling’ (side, bottom, and surface sampling)

option where the side and bottom sampling are useful for liquid samples, and surface sampling port allows for SERS measurement.

Many applications require large acquisition area and to achieve that in conventional confocal Raman Spectrometer large aperture is used to increase the laser spot size, which can effectively collect most of the scattering from the more extensive area. But increasing aperture size causes an adverse effect on resolution (small laser spot results in high resolution) as well as low signal to noise ratio, and in some cases, most of the critical information about the material is lost. This phenomenon is denoted as the 'etendue' effect. This effect is particularly problematic for rough samples like paper-based SERS substrates.

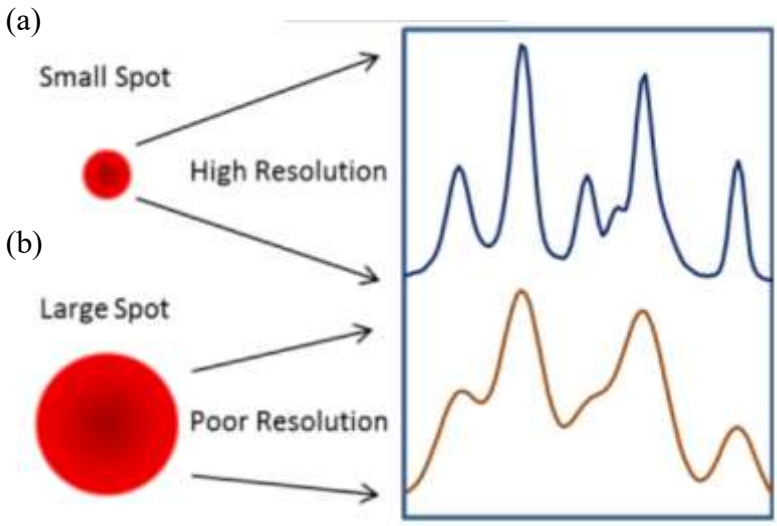

Figure 3.3 Schematic illustration of 'etendue' effect of spot size on the resolution of acquired Raman spectra. An increase in the aperture size leads to increased spot size. (a) small spot size leads to high resolution if signal collected is sufficient, (b) Large spot size leads to poor resolution and loss of molecular signature.

The portable Raman Spectrometer from SnRI uses a unique Orbital Raster Sampling (ORS) scheme to overcome issues with the etendue effect as illustrated in Figure 3.4. With the ORS option, a focused laser spot (30µm) is continuously rastered across an area having a diameter of ~2 mm on the substrate, resulting in greater sample coverage and additionally the energy density at a given point is reduced leading to a lower risk of sample degradation.

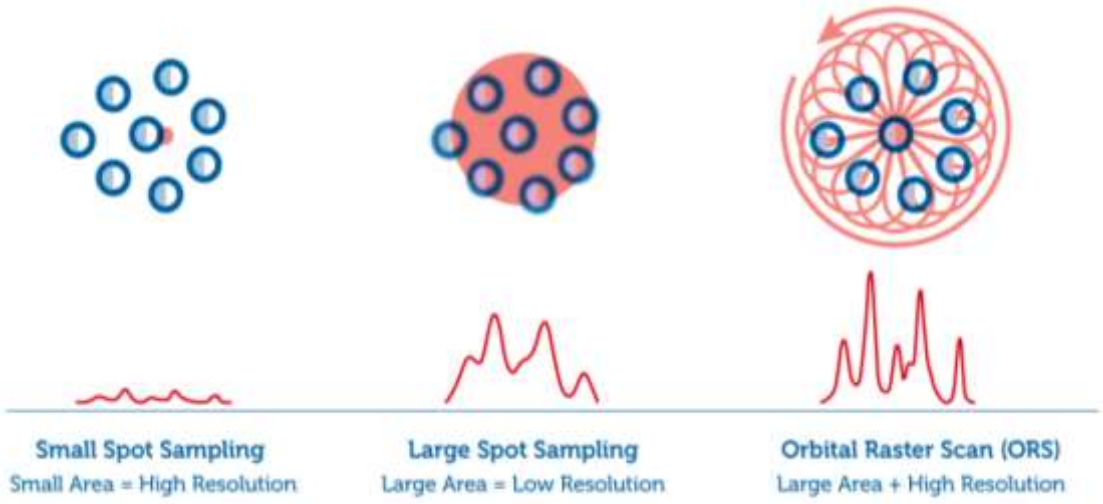

Figure 3.4 Illustration of Raman Spectra of disperse analytes. In conventional Raman Spectrometer (a) tightly focused beam might produce high resolution but it only samples a small area, (b) large spot size is produced by increasing the aperture size which leads to poor resolution, but in SnRI portable Raman Spectrometer (c) with ORS acquisition area is increased by rastering the laser spot over the surface leading to better sampling with high signal to noise ratio. (reproduced from http://www.wysri.com/apps/sers/, accessed on 10/10/2018)

Figure 3.5 shows the SERS spectra of Metanil Yellow dye, with a concentration of 1 mM, on paper-SERS substrate collected with and without ORS; it shows that the peak intensity with ORS is much higher compared to without ORS. The signal to noise ratio for 1148 peak (assigned to N=N stretching) with ORS is ~4x higher than without ORS.

3.4 Factors affecting SERS signal

The results of preliminary investigations aimed at optimizing the acquisition setup for paper-based SERS are reported in this section. The factors studied include the influence of ambient light, the distance of the substrate from the laser aperture, laser power and integration time.

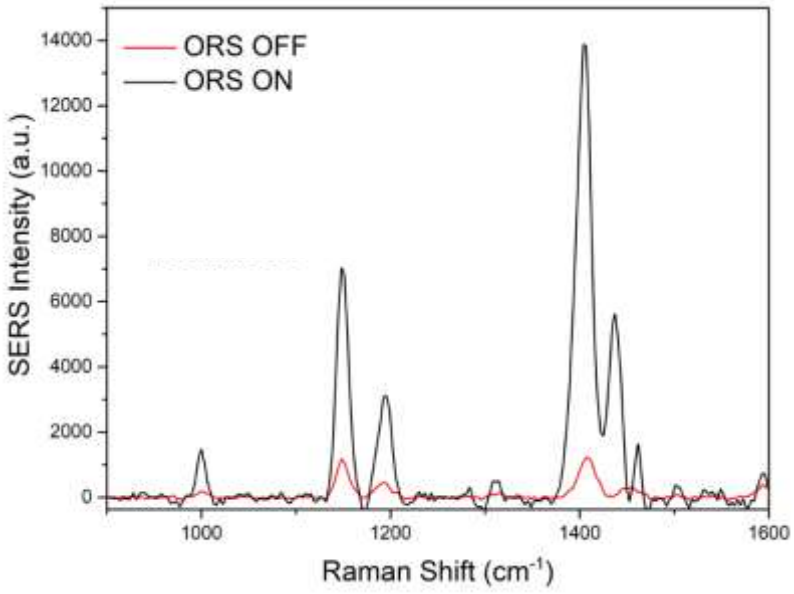

Figure 3.5 SERS spectra from SERS-swabs soaked for 12 hrs in 1 mM Metanil Yellow solution and rinsed with DI water. Comparison of spectra collected with and without ORS at 10 mW laser power and integration time 5 s.

3.4.1 Effect of ambient light

SERS signal is affected by the interference from ambient light. This factor is vital in the case of portable Raman Spectrometer because acquisition condition (ambient light) might vary from place to place. In case of low concentration of target analyte, this factor becomes significant compared to the signal of the analyte molecule and has to be corrected. The "Reference" option for background correction of ambient light interference should be switched on to overcome this problem of ambient light interference. When the reference option is ON, then the spectrometer automatically subtracts the background due to ambient light. The effect of ambient light on the SERS signal can be seen in Figure 3.6.

Figure 3.6 (a) shows the comparison between the background signal obtained from the paper-based SERS substrate without any analyte adsorbed onto it (silver nanowires on Kimwipe paper). The influence of ambient light is seen as Raman peaks at 470, 1452, 1514 cm^{-1}. With the reference option set to ON, there are no peaks in the background

signal (Figure 3.6 (b)). All the spectra acquired in this work are taken with "Reference ON" condition unless mentioned otherwise.

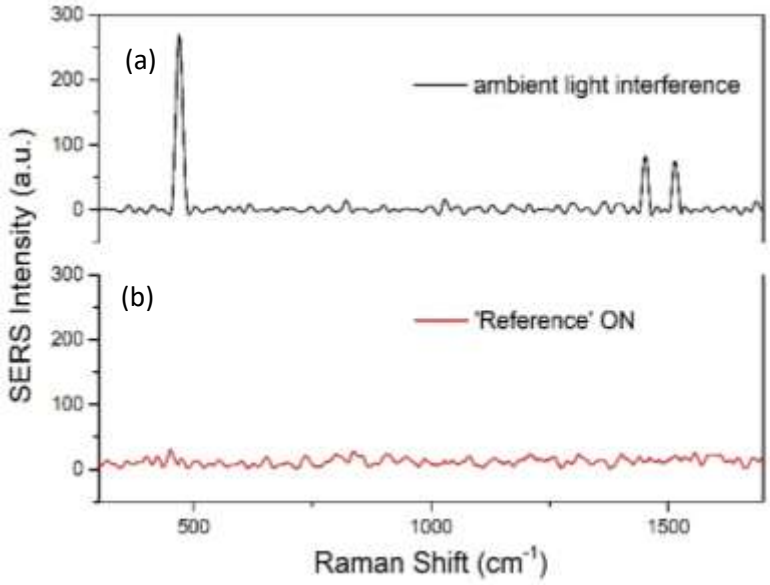

Figure 3.6 Influence of ambient light on the background spectra of SERS substrate. (a) Background SERS signal of substrate (silver nanowire on Kimwipe) without correction. The peaks present in the spectra are due to ambient light interference, (b) SERS background of substrate without the influence of ambient light. In spectra (b) Reference option is ON which has removed the influence of ambient light. Spectra acquired at 16.67 mW laser intensity and 5 s integration time with ORS in ON condition.

3.4.2 Positioning of substrate

Another critical factor which affects the SERS signal is the distance of the substrate from the laser aperture. If the substrate is too close or too far it will be out of focus, and in both these cases SERS intensity decreases as shown in Figure 3.7. So, an estimation of the position of substrate was carried out to ascertain the optimum distance of the substrate from the laser aperture. Figure 3.8 shows the change in SERS signal intensity as a function of distance from aperture for Silicon wafer and Rhodamine 6G dye on Kimwipe substrate. The positioning analysis using two different substrates shows that SERS signal intensity is maximum at an average distance of 11.4 ± 1 mm. The full width at half maximum of the SERS signal as a function of distance from the aperture

is wider for a paper-based SERS substrate (8 mm) as compared to a silicon wafer (2 mm). This difference is attributed to the following: a) the depth of penetration of the laser is negligible in the case of the silicon substrate (0.7μm for 532 nm laser [41]), and b) multiple scattering effects within the pores of the tissue paper substrate.

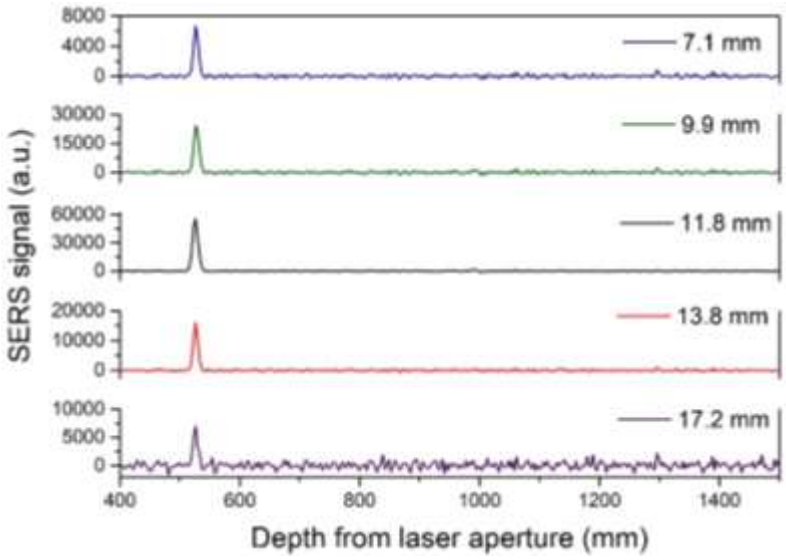

Figure 3.7 Variation of SERS signal with change in distance from laser aperture. SERS spectra are collected for Silicon wafer and target peak is 525.5 cm^{-1}. SERS spectra. Spectra acquired at 50 mW laser intensity and 5 s integration time with ORS and Reference ON conditions.

3.4.3 Effect of Laser power

SERS signal is highly dependent on the laser power. Increasing laser power increases the SERS intensity. But high laser power can also lead to CCD detector saturation due to higher fluorescence background which results in peak cut-off (Figure 3.11). Figure 3.11 shows that increasing laser power leads to high peak intensity but after 23.33 mW laser power CCD detector saturates and the signal is cut-off. Visually, another effect of high laser power can be seen in Figure 3.9, where lighter circles on the substrate indicate a change in colour of the substrate after exposure to high laser power.

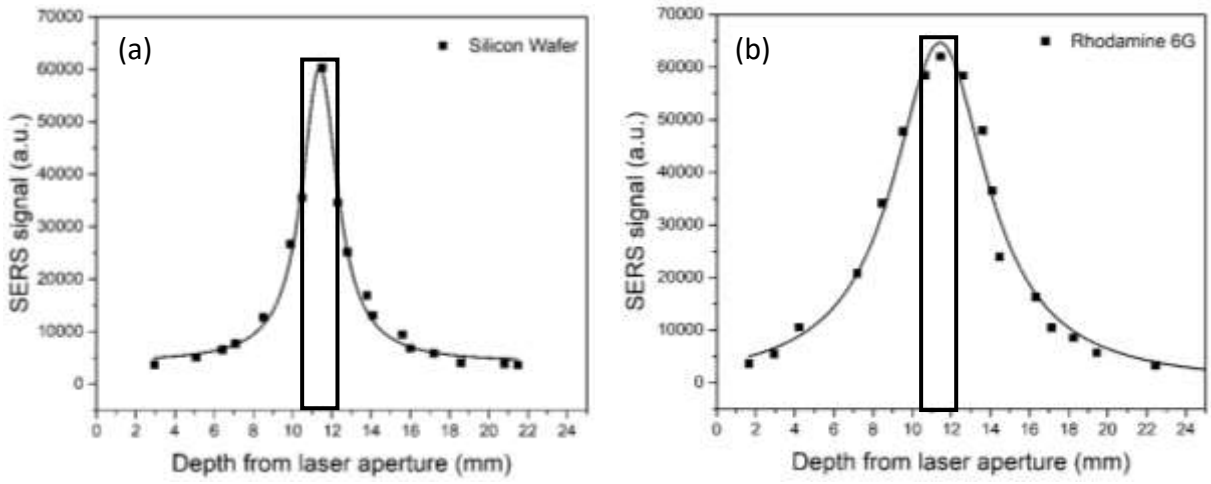

Figure 3.9 SERS signal as a function of distance of the substrate from the laser aperture for (a) Silicon substrate (525.5 cm^{-1} peak), and (b) Rhodamine 6G (R6G) dye (616 cm^{-1} peak) adsorbed on paper-SERS substrate. The maximum intensity for Silicon and R6G is achieved in the range 11.4 ± 1 mm from laser aperture. SERS signal were acquired at (a) 50 mW laser intensity and for integration time of 5 s, and (b) 3.33 mW laser intensity and for integration time of 1 s, with ORS and Reference ON conditions. Data points were fitted with a Lorentz curve.

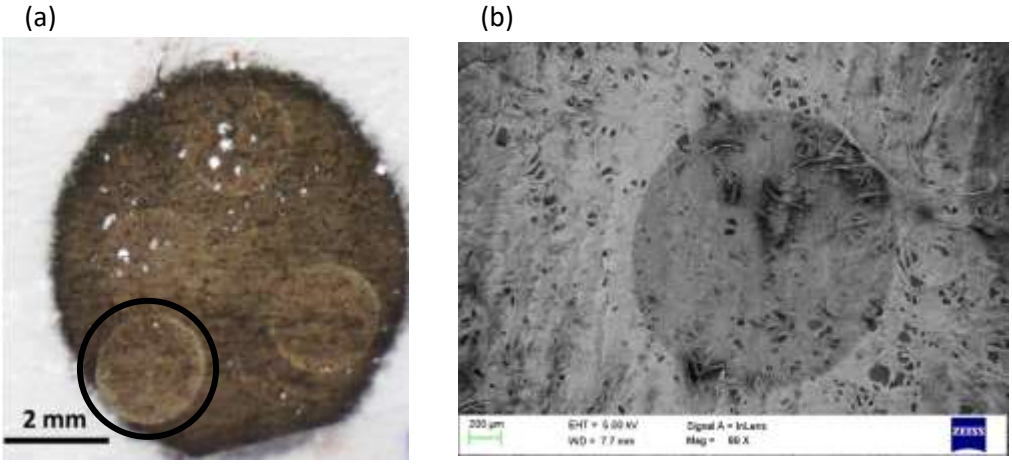

Figure 3.8 Image showing the effect of high laser power on the nanowire substrate. (a) High laser power has led to a change in the colour of the substrate, as visible in the encircled area. (b) FESEM image of the affected area, clear colour distinction can be made. Dark area is the affected area on the substrate.

(a) (b)

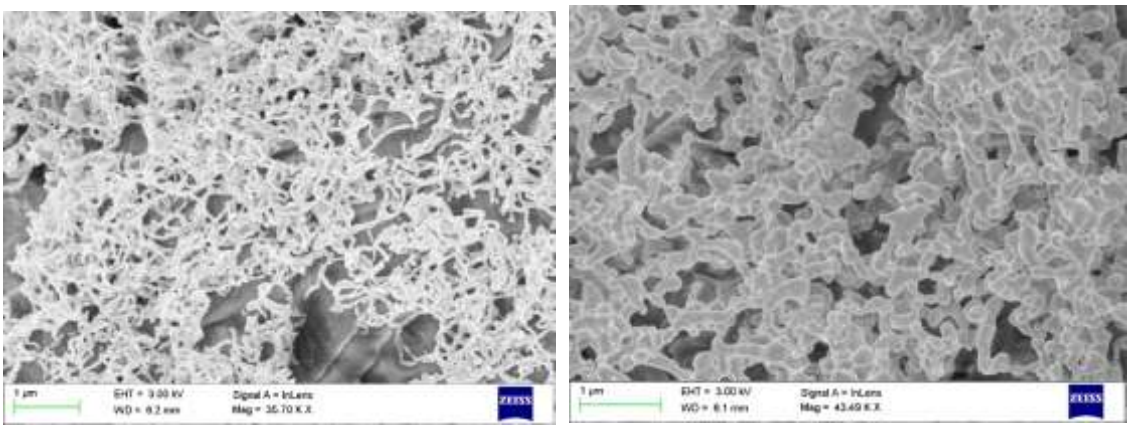

Figure 3.11 FESEM image of the (a) non-affected area, (b) laser affected area

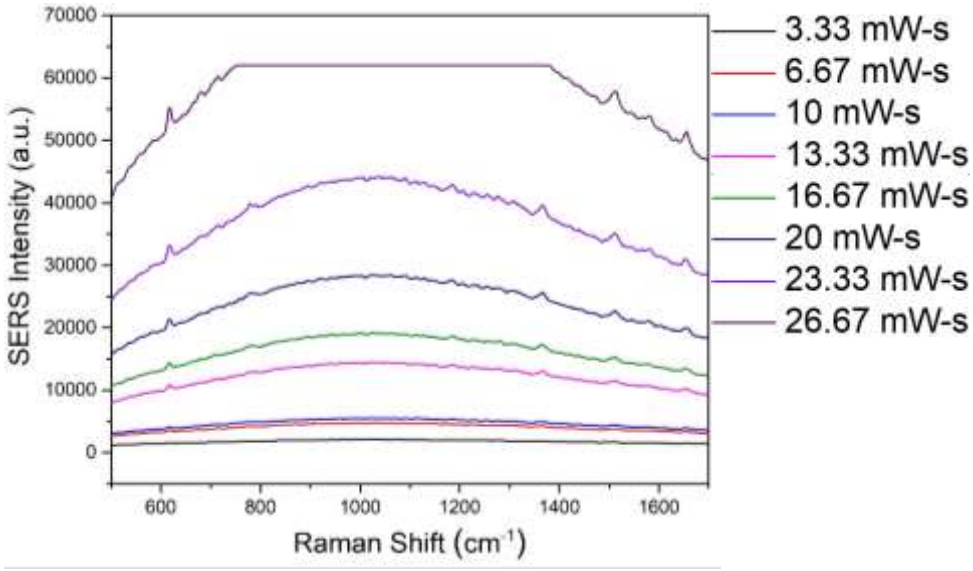

Figure 3.10 Variation of SERS spectra with laser power for paper-SERS substrate soaked in Rhodamine 6G solution having concentration of 10 µM. Spectra were acquired using varied laser intensity and 1 s integration time with ORS and Reference ON conditions.

This change in colour is attributed to a change in nanostructure morphology due to high laser intensity. FESEM image of laser affected area on substrate shows the change in the morphology of the nanostructures due to fusion and coarsening to form plate-like structures (Figure 3.10). Dissociation of the target molecule is also possible at high laser power. So, to avoid CCD detector saturation and any risk of damage to the paper

substrate or analyte due to high laser power, the laser power is maintained < 20 mW for all the results reported hereafter.

3.4.4 Effect of integration time

The integration time is another factor that can affect the signal to noise ratio. A linear increase in the 525.5 cm^{-1} peak intensity from a silicon substrate with increasing integration time is observed (Figure 3.12). To avoid any potential risk due to longer duration of acquisition the minimum time (2-5 s) required for acquiring spectra with good signal to noise ratio is used for paper-based substrates. Notably, the expectation that higher dosage (i.e. Laser power intensity x Integration time) should affect substrate damage is not valid here. This is because, with the ORS on, there is very little chance of the 30 µm spot revisiting the same area within the 2 mm diameter signal collection area. So, the Laser intensity is the critical factor with ORS in the ON state.

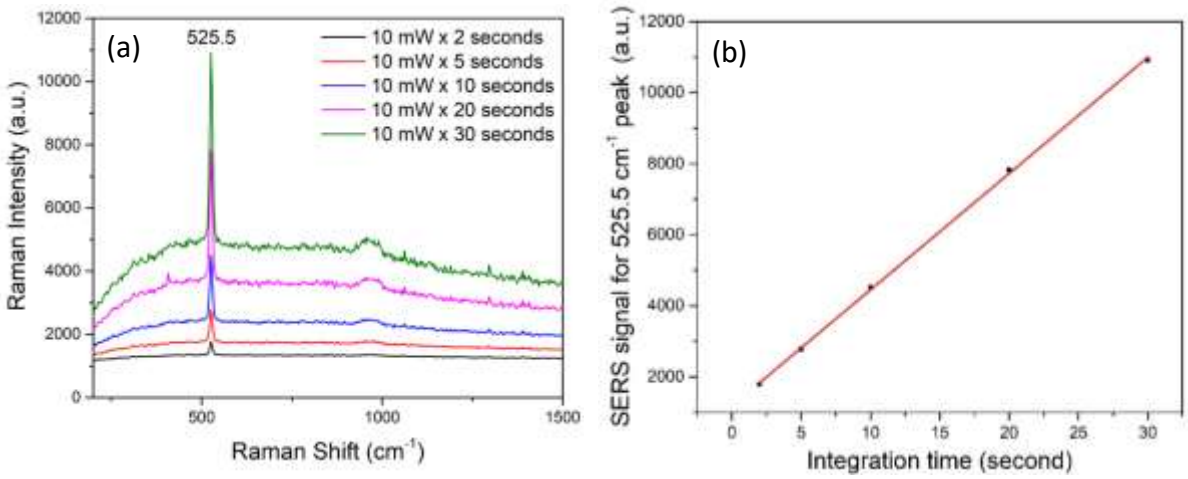

Figure 3.12 Effect of integration time on Raman spectra of silicon substrate, (b) Signal intensity increases linearly with integration time. Spectra acquired at 10 mW laser intensity and variable integration time with ORS and Reference ON conditions.

3.4.5 SERS signal variation across substrates

To estimate the reproducibility of the fabrication process and repeatability of SERS signals the performance of three samples, consisting of paper-based SERS substrates with a nominal silver loading of 1 mg/cm^2 soaked overnight in 1 mM solutions of R6G

in water, were characterized. This procedure ensures that there is a complete coverage of R6G molecules on the silver substrate and that any variation detected is attributable to variability of the average signal enhancements within and across different substrates. Figure 3.13 (c) shows that the SERS signals with ORS ON are within 1.6% of the average value both within a substrate as well across the three substrates. This robust response despite the microscale non-uniformity of the silver nanostructures and surface roughness of the paper substrate is attributed to the larger interrogation areas (~ 2 mm) used (Figure 3.13 (a)). At this length scale, the paper-based SERS substrate appears to be macroscopically uniform (Figure 3.13 (b)). To verify this hypothesis, SERS signals were collected with the ORS function turned off. The variation in the signal is observed to be 10%, which is similar to the value reported earlier (7) for such paper-based substrates, with the earlier data being obtained using a confocal Raman spectrometer and a 1 µm spot size.

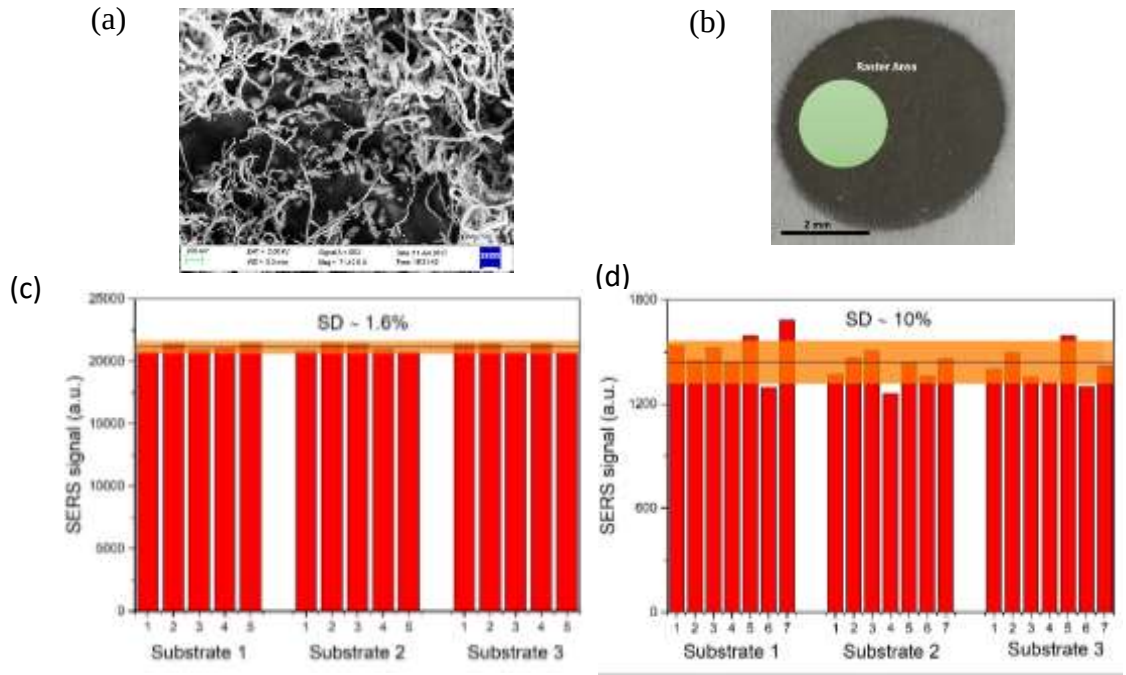

Figure 3.13 Reproducibility of SERS signal within and across the substrates. (a) FESEM image of Kimwipe substrate showing the morphology of silver nanowires, (b) comparison of size of Raster area and SERS substrate area. Overall variation of SERS signal of 616 cm^{-1} peak integrated area for 1 mM R6G across all the substrates (c) 1.6 % SD in SERS signal with ORS ON condition and (d) 10 % SD in SERS signal with ORS OFF condition. Spectra acquired at 10 mW laser intensity and 1 s integration time with Reference ON condition. The orange bands represent average ± SD and are an aid to the eye.

3.5 SERS detection capability

SERS signals were obtained from Rhodamine 6G (R6G), Malachite Green Oxalate (MG), and Metanil Yellow (MY) dyes adsorbed onto Kimwipe substrate from aqueous solutions with concentrations ranging from 1 pM to 1 mM. The substrates were soaked in appropriate aqueous solutions of dye for 12 h and then rinsed with water. Physically adsorbed molecules are expected to be removed after rinsing with DI water, leaving a chemically adsorbed layer on top of the silver nanostructures. The surface coverage density of the dye molecules is related to the bulk concentration of the solutions via adsorption isotherms. Typically [7], Langmuir isotherm is used to account for the sigmoidal shape (see Figure 3.15) of the SERS signal vs bulk concentration data, implicitly assuming that the SERS signal is directly proportional to the surface coverage density. Given the acute sensitivity of SERS effect to the first adsorbed monolayer, the Langmuir model fits the data satisfactorily at or near saturation but deviates from it at lower values. The deviation in the SERS signal is attributed to the plasmonic 'hotspots'.

In the following sections, a brief introduction to Langmuir is provided, following this an analysis of the measured data for three different dyes, namely Rhodamine 6G, Malachite Green Oxalate, and Metanil yellow are provided.

3.5.1 Langmuir isotherm

The Langmuir isotherm model is based on the following assumptions:

- The adsorbent's surface is homogeneous
- Surface diffusion of adsorbate is negligible
- All 'sites' for adsorption are equivalent in terms of energetics
- The interaction between adsorbed molecules is negligible
- The SERS intensity is linearly proportional to the number of adsorbed molecules

Based on these assumptions, the Langmuir adsorption isotherm is stated as [42], [43]:

$$I_e = \frac{I_m\, C_e}{1/_{K_e} + C_e} \tag{4.1}$$

C_e: adsorbate concentration at equilibrium

I_e: SERS signal in equilibrium with Ce

Ke: adsorption equilibrium constant

I_m: saturating SERS intensity

3.5.2 Adsorption analysis of Rhodamine 6G on silver nanowires

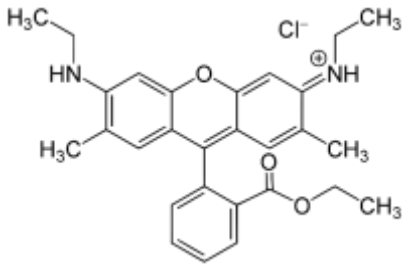

Figure 3.14 Molecular structure of Rhodamine 6G dye.

The adsorption analysis of R6G dye (molecular structure is shown in Figure 3.14) on paper-based silver nanowire substrate was performed using a portable Raman Spectrometer equipped with 532 nM laser. A representative set of spectra obtained are shown in appendix A. The integrated area of peak 1510 cm^{-1} (pertaining to aromatic C–H bending mode [44]) is plotted against the corresponding R6G solution concentration in semi-log plot and exhibits a sigmoidal shape (Figure 3.15). For the adsorption of R6G onto silver, Langmuir adsorption fit provide $1/K_e \cong 2.1 \times 10^{-6}$; which leads to adsorption energy $\cong$ RT ln(K_e) $\cong$ 32.6 KJ/mol, which is significantly close to the value of 36 KJ/mol reported in the literature [45].

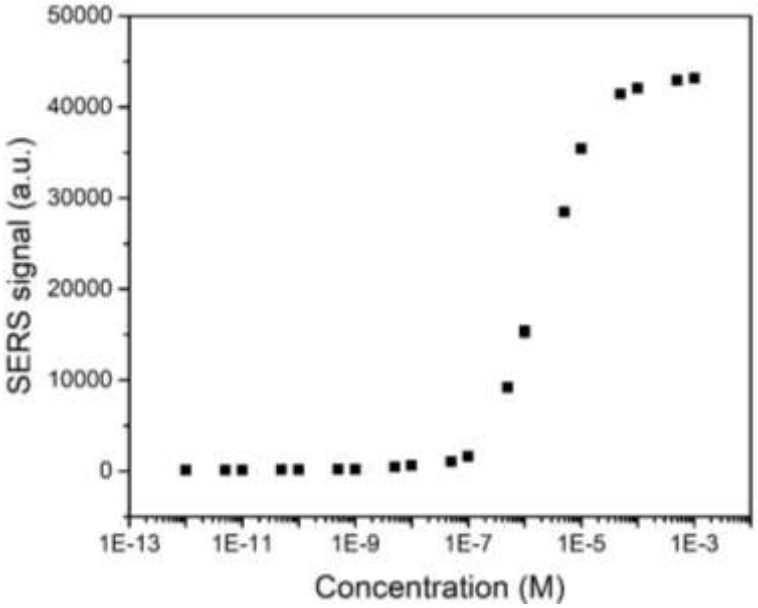

Figure 3.15 SERS signals corresponding to 616 cm^{-1} peak's integrated area plotted against respective R6G concentrations. Spectra were acquired using a 3.33 mW laser power and 1 s integration time with ORS and Reference ON conditions. The error bars correspond to SERS signal variation within the substrate.

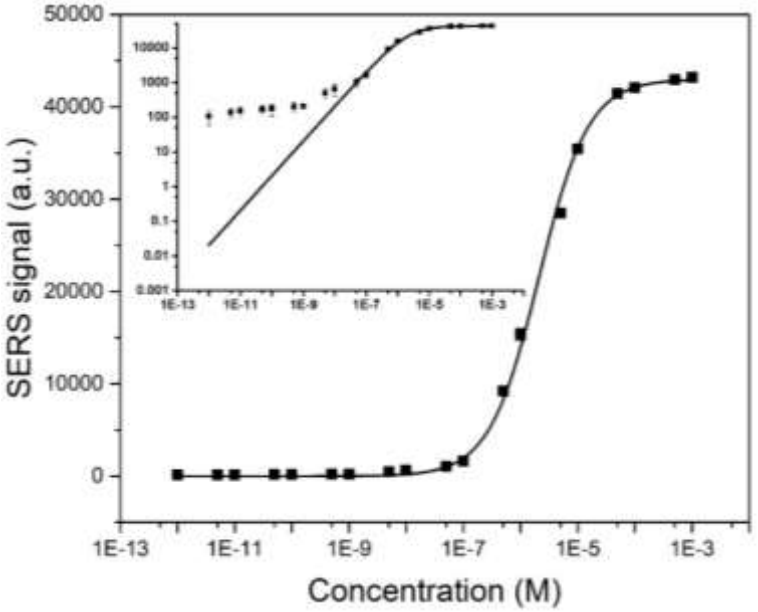

Figure 3.16 Langmuir Isotherm fir for Rhodamine 6G dye. Inset shows a log-log plot highlighting the difference between data and model at lower concentrations.

The Langmuir isotherm fits the experimental data collected by portable Raman spectrometer much better at higher solution concentrations compared to lower concentrations as shown in Figure 3.16 inset. The Raman signal predicted by the Langmuir isotherm is lower than the acquired Raman signal. We ascribe this higher Raman signal measured as compared to the value predicted by Langmuir isotherm to plasmonic 'hotspots', which leads to a breakdown in the assumption of uniform adsorption sites. The minimum concentration of R6G detected here is 10^{-11} M using paper-based SERS substrates, whereas concentration down to 10^{-12} M have been detected using a confocal Raman microscope [7].

3.5.3 Adsorption analysis of Malachite Green Oxalate on silver nanowires

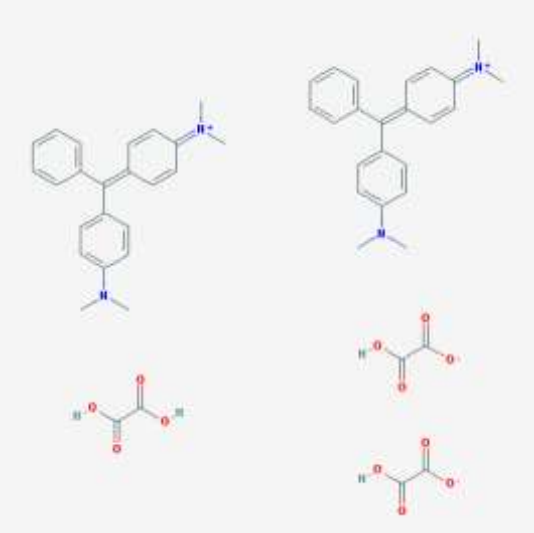

Figure 3.17 Molecular structure of Malachite Green Oxalate dye.

The concentration-based adsorption analysis of Malachite Green Oxalate dye was carried out by soaking the SERS silver substrate into the aqueous dye solution of varying concentration from 1 mM to 100 pM for 12 hrs and rinsing thoroughly with DI water. A representative set of spectra obtained are shown in appendix A. The integrated area of peak 1370 cm^{-1} (pertaining to N-phenyl stretching [46]) is plotted against the corresponding MG Oxalate solution concentration in semi-log plot and exhibits a

sigmoidal shape similar to R6G (Figure 3.18). Langmuir adsorption fit provides a value of $1/K_e \cong 2.74 \times 10^{-6}$; which leads to adsorption energy $\cong RT \ln(K_e) \cong 31.94$ KJ/mol.

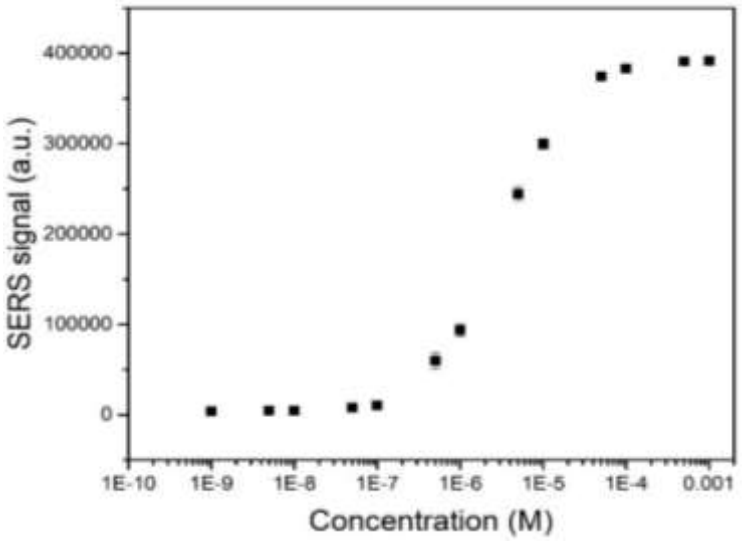

Figure 3.18 SERS signals corresponding to 1370 cm^{-1} peak's integrated area plotted against respective MG Oxalate concentrations. Spectra were acquired using a 16.67 mW laser power and 5 s integration time with ORS and Reference ON conditions. The error bars correspond to SERS signal variation within the substrate.

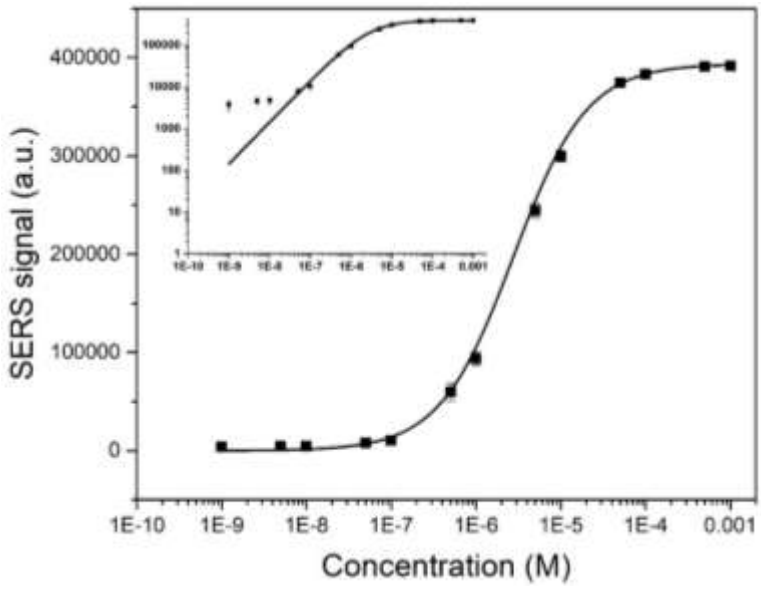

Figure 3.19 Langmuir Isotherm fir for Malachite Green Oxalate dye. Inset shows a log-log plot highlighting the difference between data and model at lower concentrations.

Similar to R6G, the Langmuir isotherm fits the experimental data collected by portable Raman spectrometer much better at higher solution concentrations compared to lower concentrations as shown in Figure 3.19 inset. This result is also attributed to the presence of hotspots. The minimum concentration of MG oxalate detected here is 10^{-9} M, whereas earlier studies has reported up to $2.74x10^{-9}$ level of detection [47].

3.5.4 Adsorption analysis of Metanil Yellow on silver nanowires

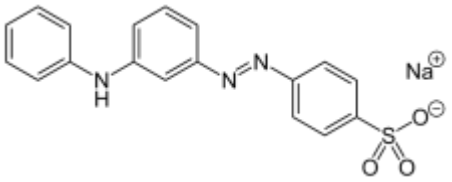

Figure 3.21 Molecular structure of Metanil Yellow.

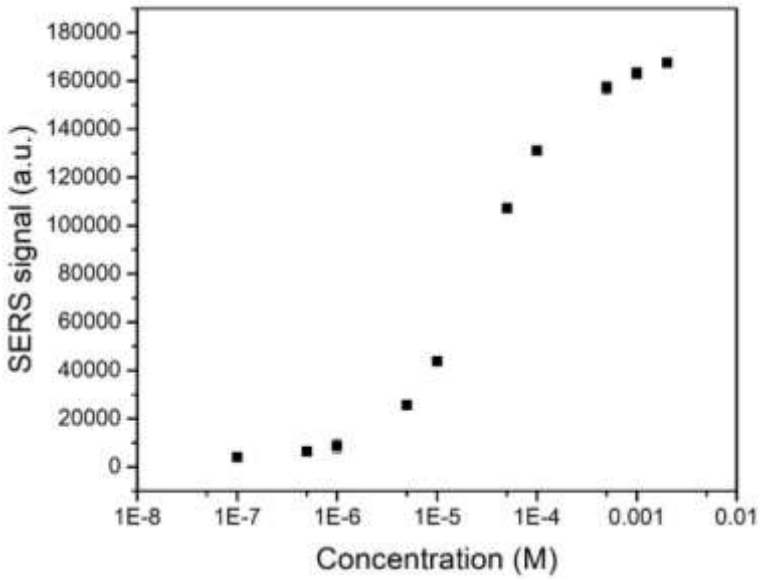

Figure 3.20 SERS signals corresponding to 1148 cm^{-1} peak's integrated area plotted against respective MY concentrations. Spectra were acquired using a 16.67 mW laser power and 5 s integration time with ORS and Reference ON conditions. The error bars correspond to SERS signal variation within the substrate.

SERS spectra of Metanil Yellow are collected from the substrate soaked in the dye solution for 12 hrs and then rinsed with the DI water. The concentration-based adsorption analysis was carried out for Metanil Yellow (MY) dye too. A representative set of spectra obtained are shown in appendix A. The integrated area under the peak at 1148 cm^{-1} (ν (C-N_{azo}) stretching) is plotted against the corresponding solution concentration of MY, which exhibits a sigmoidal shape (Figure 3.21). Langmuir adsorption fit provide $1/K_e \cong 2.81 \times 10^{-5}$; which leads to adsorption energy ≅ RT ln(K_e) ≅ 26.138 KJ/mol. Similar to R6G and MG Oxalate, the Raman signal predicted by the Langmuir isotherm is lower than the acquired Raman signal. On the basis of R6G, MG Oxalate, and MY, it can be concluded that at lower concentration range SERS signal predicted by Langmuir isotherm deviates negatively, and it can be attributed to the presence of 'hotspots' onto the SERS substrate. The minimum concentration of MY detected in this work is 10^{-7} M, whereas detection up to 10^{-14} M concentration has been reported using a 438 nm laser source [48].

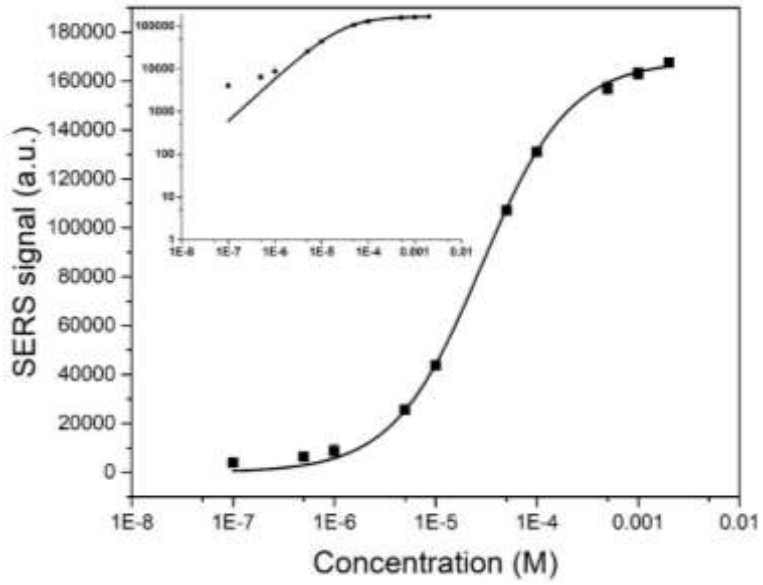

Figure 3.22 Langmuir Isotherm fir for Metanil Yellow dye. Inset shows a log-log plot highlighting the difference between data and model at lower concentrations.

To summarize the adsorption data collected by the Portable Raman Spectrometer, trends for Rhodamine 6G, Malachite Green Oxalate, and Metanil Yellow dyes are similar. Adsorption analysis shows that Langmuir isotherm fits well at higher concentration range due to the uniform distribution of analyte molecules over the surface of Kimwipe SERS substrate. But at lower concentration predicted SERS signal by Langmuir isotherm is lower than the acquired experimental data, and we attribute these heterogenous 'active' adsorption sites to the presence of hotspots. However, the SERS response is well-captured by Langmuir-isotherm based fits over the concentration range of interest for practical applications, as the lower concentrations are too dilute to effectively enhance the appearance of food.

In this chapter, we have discussed the effect of the laser spot and how the size of laser spot affected the SERS signal and reviewed the use of *Orbital Raster Sampling (ORS)* to overcome the problem of 'etendue' effect. Then we discussed the interference due to ambient light on the SERS signal and how a *'Reference'* is needed. To get the best spectra positioning of substrate analysis was discussed to show the effect of distance of the substrate from the laser aperture on the SERS signal. The results show that 11.4 ± 1 mm is the optimum distance of the substrate from the laser aperture. Then the effect of laser power on the SERS signal and on the substrate was discussed, which shows that high laser power leads to detector saturation and can also change the morphology of the silver nanostructures. The analysis of Rhodamine 6G dye on Kimwipe substrate shows that 10 mW is the optimum laser power for SERS analysis using a portable Raman Spectrometer. Analysis of the effect of integration time on SERS signal was done using a Silicon wafer, which shows the linear increase in the SERS signal with integration time. To avoid any risk of damage 2-5 s integration time was selected. Then we moved to analyse the uniformity of the SERS substrate. The low value of SERS signal variation (CV of 1.6%) for Rhodamine 6G dye shows that the signal can be averaged over 3-4 spots within a substrate as well as across substrates attesting to the uniform nature of the silver nanostructures and reproducibility of the fabrication process. Further, after optimizing the acquisition conditions of Portable Raman Spectrometer, the detection capability of Spectrometer was tested using concentration-based adsorption SERS analysis. The Langmuir isotherm model is found to fit the

adsorption data well at concentrations of interest and the corresponding values estimated for the adsorption energies agree well with reported values. The adsorption analysis also shows that at very low concentration SERS signal predicted by the Langmuir isotherm is lower than the actual SERS signal which is attributed to the effect of hotspots. The following chapter covers the detection of adulterants from intentionally-adulterated food samples to ascertain the detection capability of SERS swabs with Portable Raman Spectrometer. Then real-world samples of green chillies, green peas, and dals from various stores will be tested to check for the presence of adulterants.

REFERENCES

[1] M. Fleischmann, P. J. Hendra, and A. J. McQuillan, "Raman spectra of pyridine adsorbed at a silver electrode," *Chem. Phys. Lett.*, vol. 26, no. 2, pp. 163–166, May 1974.

[2] D. L. Jeanmaire and R. P. Van Duyne, "Surface raman spectroelectrochemistry: Part I. Heterocyclic, aromatic, and aliphatic amines adsorbed on the anodized silver electrode," *J. Electroanal. Chem. Interfacial Electrochem.*, vol. 84, no. 1, pp. 1–20, Nov. 1977.

[3] K. Kneipp *et al.*, "Single Molecule Detection Using Surface-Enhanced Raman Scattering (SERS)," *Phys. Rev. Lett.*, vol. 78, no. 9, pp. 1667–1670, Mar. 1997.

[4] S. Dhakal, K. Chao, W. Schmidt, J. Qin, M. Kim, and Q. Huang, "Detection of Azo Dyes in Curry Powder Using a 1064-nm Dispersive Point-Scan Raman System," *Appl. Sci.*, vol. 8, no. 4, p. 564, Apr. 2018.

[5] K. Chao, S. Dhakal, J. Qin, M. Kim, and Y. Peng, "A 1064 nm Dispersive Raman Spectral Imaging System for Food Safety and Quality Evaluation," *Appl. Sci.*, vol. 8, no. 3, p. 431, Mar. 2018.

[6] S. Guest and E. Section, "Inedible Azo Dyes and Their Analytical Methods in Foodstuffs and Beverages," 2018.

[7] P. Joshi and V. Santhanam, "Paper-based SERS active substrates on demand," *RSC Adv.*, vol. 6, no. 72, pp. 68545–68552, 2016.

[8] A. Hakonen, P. O. Andersson, M. Stenbæk Schmidt, T. Rindzevicius, and M. Käll, "Explosive and chemical threat detection by surface-enhanced Raman scattering: A review," *Anal. Chim. Acta*, vol. 893, pp. 1–13, 2015.

[9] W. Sers, "P - SERS ™ Technology Technical Paper P-SERS ™ — Trace detection overcoming the cost and usability limitations of traditional SERS technology," pp. 1–8, 2015.

[10] C. Muehlethaler, M. Leona, and J. R. Lombardi, "Review of Surface Enhanced Raman Scattering Applications in Forensic Science," *Anal. Chem.*, vol. 88, no. 1, pp. 152–169, 2016.

[11] Karen E. Shafer-Peltier, Christy L. Haynes, and Matthew R. Glucksberg, and ‡ Richard P. Van Duyne, "Toward a Glucose Biosensor Based on Surface-Enhanced Raman Scattering," 2002.

[12] Lili Bao, S. M. Mahurin, and R. G. Haire, and S. Dai, "Silver-Doped Sol−Gel Film as a Surface-Enhanced Raman Scattering Substrate for Detection of Uranyl and Neptunyl Ions," 2003.

[13] Shawn P. Mulvaney, Michael D. Musick, and Christine D. Keating, and M. J. Natan, "Glass-Coated, Analyte-Tagged Nanoparticles: A New Tagging System Based on Detection with Surface-Enhanced Raman Scattering," 2003.

[14] W. E. D. and and S. Nie, "Spectroscopic Tags Using Dye-Embedded Nanoparticles and Surface-Enhanced Raman Scattering," 2003.

[15] Y. C. Cao, R. Jin, and C. A. Mirkin, "Nanoparticles with Raman spectroscopic fingerprints for DNA and RNA detection.," *Science*, vol. 297, no. 5586, pp. 1536–40, Aug. 2002.

[16] Roger M. Jarvis, and Alan Brooker, and Royston Goodacre, "Surface-Enhanced Raman Spectroscopy for Bacterial Discrimination Utilizing a Scanning Electron Microscope with a Raman Spectroscopy Interface," 2004.

[17] R. M. Connatser *et al.*, "Toward Surface-Enhanced Raman Imaging of Latent Fingerprints," *J. Forensic Sci.*, vol. 55, no. 6, pp. 1462–1470, Nov. 2010.

[18] L. Polavarapu and L. M. Liz-Marzán, "Towards low-cost flexible substrates for nanoplasmonic sensing," *Phys. Chem. Chem. Phys.*, vol. 15, no. 15, p. 5288, Mar. 2013.

[19] G. Sauer, U. Nickel, and S. Schneider, “Preparation of SERS-active silver film electrodes via electrocrystallization of silver,” *J. RAMAN Spectrosc. J. Raman Spectrosc*, vol. 31, pp. 359–363, 2000.

[20] “Practical substrate and apparatus for static and continuous monitoring by surface-enhanced raman spectroscopy,” May 1985. https://patents.google.com/patent/US4674878A/en (accessed July 10, 2018).

[21] G. Xue, Y. Lu, and J. Zhang, “Stable SERS Substrates Used for In Situ Studies of the Polymer-Metal Interface at Elevated Temperature,” *Macromolecules*, vol. 27, pp. 809–813, 1994.

[22] B. R. Martin *et al.*, “Orthogonal Self-Assembly on Colloidal Gold-Platinum Nanorods,” *Adv. Mater.*, vol. 11, no. 12, pp. 1021–1025, Aug. 1999.

[23] M. Sackmann and A. Materny, “Surface enhanced Raman scattering (SERS)—a quantitative analytical tool,” *J. Raman Spectrosc.*, vol. 37, no. 1–3, pp. 305–310, Jan. 2006.

[24] Jiatao Zhang, Xiaolin Li, and Xiaoming Sun, and Y. Li, “Surface Enhanced Raman Scattering Effects of Silver Colloids with Different Shapes,” 2005.

[25] V. S. Tiwari, T. Oleg, G. K. Darbha, W. Hardy, J. P. Singh, and P. C. Ray, “Non-resonance SERS effects of silver colloids with different shapes,” *Chem. Phys. Lett.*, vol. 446, no. 1–3, pp. 77–82, Sep. 2007.

[26] M. J. Mulvihill, X. Y. Ling, J. Henzie, and P. Yang, “Anisotropic Etching of Silver Nanoparticles for Plasmonic Structures Capable of Single-Particle SERS,” *J. Am. Chem. Soc.*, vol. 132, no. 1, pp. 268–274, Jan. 2010.

[27] K. L. Wustholz *et al.*, “Structure−Activity Relationships in Gold Nanoparticle Dimers and Trimers for Surface-Enhanced Raman Spectroscopy,” *J. Am. Chem. Soc.*, vol. 132, no. 31, pp. 10903–10910, Aug. 2010.

[28] Y. H. Ngo, D. Li, G. P. Simon, and G. Garnier, “Gold Nanoparticle–Paper as a Three-Dimensional Surface Enhanced Raman Scattering Substrate,” *Langmuir*, vol. 28, no. 23, pp. 8782–8790, Jun. 2012.

[29] C. H. Lee, M. E. Hankus, L. Tian, P. M. Pellegrino, and S. Singamaneni, “Highly Sensitive Surface Enhanced Raman Scattering Substrates Based on Filter Paper Loaded

with Plasmonic Nanostructures," *Anal. Chem.*, vol. 83, no. 23, pp. 8953–8958, Dec. 2011.

[30] W. Zhang *et al.*, "Brushing, a simple way to fabricate SERS active paper substrates," *Anal. Methods*, vol. 6, no. 7, pp. 2066–2071, Mar. 2014.

[31] Z. Gong, H. Du, F. Cheng, C. Wang, C. Wang, and M. Fan, "Fabrication of SERS Swab for Direct Detection of Trace Explosives in Fingerprints," *ACS Appl. Mater. Interfaces*, vol. 6, no. 24, pp. 21931–21937, Dec. 2014.

[32] S. K. Sivaraman and V. Santhanam, "Realization of thermally durable close-packed 2D gold nanoparticle arrays using self-assembly and plasma etching," *Nanotechnology*, vol. 23, no. 25, p. 255603, Jun. 2012.

[33] L.-L. Qu, D.-W. Li, J.-Q. Xue, W.-L. Zhai, J. S. Fossey, and Y.-T. Long, "Batch fabrication of disposable screen printed SERS arrays," *Lab Chip*, vol. 12, no. 5, pp. 876–881, Feb. 2012.

[34] W. W. Yu and I. M. White, "Inkjet Printed Surface Enhanced Raman Spectroscopy Array on Cellulose Paper," *Anal. Chem.*, vol. 82, no. 23, pp. 9626–9630, Dec. 2010.

[35] W. W. Yu and I. M. White, "Inkjet-printed paper-based SERS dipsticks and swabs for trace chemical detection," *Analyst*, vol. 138, no. 4, pp. 1020–1025, Jan. 2013.

[36] Y. Zhu, M. Li, D. Yu, and L. Yang, "A novel paper rag as 'D-SERS' substrate for detection of pesticide residues at various peels," *Talanta*, vol. 128, pp. 117–124, Oct. 2014.

[37] M. Volkan, D. L. Stokes, and T. Vo-Dinh, "A sol–gel derived AgCl photochromic coating on glass for SERS chemical sensor application," *Sensors Actuators B Chem.*, vol. 106, no. 2, pp. 660–667, May 2005.

[38] S. K. Parmar and V. Santhanam, "In situ formation of silver nanowire networks on paper," *Curr. Sci.*, vol. 107, no. 2, pp. 262–268, 2014.

[39] J. F. Hamilton, "The silver halide photographic process," *Adv. Phys.*, vol. 37, no. 4, pp. 359–441, Aug. 1988.

[40] S. G. Anchell, *The darkroom cookbook*. Focal Press, 2008.

[41] F. Adar, "Depth Resolution of the Raman Microscope: Optical Limitations and Sample

Characteristics," *Spectroscopy*, 2010.

[42] I. Langmuir, "The Adsorption Of Gases On Plane Surfaces Of Glass, Mica And Platinum.," *J. Am. Chem. Soc.*, vol. 40, no. 9, pp. 1361–1403, Sep. 1918.

[43] H. K. Boparai, M. Joseph, and D. M. O'Carroll, "Kinetics and thermodynamics of cadmium ion removal by adsorption onto nano zerovalent iron particles," *J. Hazard. Mater.*, vol. 186, no. 1, pp. 458–465, Feb. 2011.

[44] E. P. Hoppmann, W. W. Yu, and I. M. White, "Highly sensitive and flexible inkjet printed SERS sensors on paper," *Methods*, vol. 63, no. 3, pp. 219–224, Oct. 2013.

[45] P. Hildebrandt and M. Stockburger, "Surface-enhanced resonance Raman spectroscopy of Rhodamine 6G adsorbed on colloidal silver," *J. Phys. Chem.*, vol. 88, no. 24, pp. 5935–5944, Nov. 1984.

[46] L. He, N.-J. Kim, H. Li, Z. Hu, and M. Lin, "Use of a Fractal-like Gold Nanostructure in Surface-Enhanced Raman Spectroscopy for Detection of Selected Food Contaminants."

[47] G. H. Seong *et al.*, "Fast and sensitive trace analysis of malachite green using a surface-enhanced Raman microfluidic sensor," *Anal. Chim. Acta*, vol. 590, no. 2, pp. 139–144, 2007.

[48] Y. Kalachyova *et al.*, "Large-Scale, Ultrasensitive, Highly Reproducible and Reusable Smart SERS Platform Based on PNIPAm-Grafted Gold Grating," *ChemNanoMat*, vol. 3, no. 2, pp. 135–144, 2016.

Chapter 4 Direct detection of the adulteration of dals and vegetables with organic dyes

4.1 Introduction

Food adulteration is an act of degrading the quality of food items for profit. A commonly reported form of adulteration is the colouring of foodstuff using organic dyes to enhance the appeal or to make old stock appear fresh. This chapter reports the results of experiments conducted for swab-based direct detection of organic dyes, namely Metanil Yellow on dals and Malachite Green Oxalate from the skins of green peas and green chillies. Following this, the efficacy of some remedies commonly available in the marketplace is characterized.

Food Safety and Standards Authority of India (FSSAI) has reported the overall increase in food adulteration from 13% to 23% from 2011 to 2017. The frequency of use of Metanil Yellow on dals and Malachite Green Oxalate on green vegetables is reported to be 3.5% and 1.25 % respectively [1]. Some specific studies have reported the presence of Metanil Yellow in dals in Mysore [2] and Andhra Pradesh [3]. For the detection of Metanil Yellow, FSSAI suggests a simple indicator test with HCl, wherein when concentrated HCl is added to a dal sample the colour of the solution will turn pink if and only if the dal is coated with Metanil Yellow (Figure 4.1).

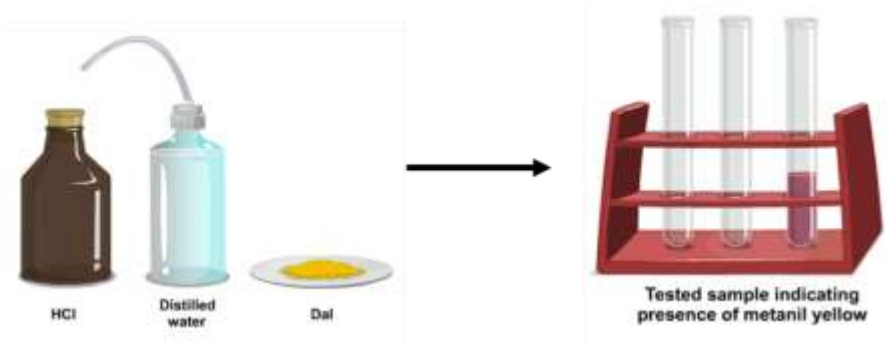

Figure 4.1 Cartoon of FSSAI suggested test for Metanil Yellow detection from dals

4.2 Limit of detection of FSSAI suggested test for Metanil Yellow

For the preparation of dal samples adulterated with a known amount of dye, Toor dal, procured from an organic outlet, was used as the starting material. Sample preparation of adulterated dals involved the spraying of 130 µL of aqueous Metanil Yellow solution of known concentration on 20 mg of dals spread in a container and drying it overnight. A mini perfume atomizer was used for spraying to mimic real-world spraying conditions. The bulk concentration of Metanil Yellow was varied in the range of 1 mM to 10 nM. Soaking of dal samples in solutions was avoided as that leads to excessive bloating of the dal samples and defeats the purpose of adulteration. FSSAI suggested HCl test was performed on all the samples. The presence of Metanil Yellow was indicated by the appearance of pink colour for the samples adulterated using 1 mM solution. But this test fails for the samples adulterated using solutions having concentration 100 µM and lower (Figure 4.2). Dals adulterated with 100 µM and lower appear like non-adulterated dal (*vide infra*) available in the marketplace. This opens the possibility of adulteration in that range ($\leq$ 10 µM) as it cannot be easily detected by the FSSAI suggested quick diagnostic test.

4.3 Detection using SERS – efficacy of swabbing

The failure of the simple diagnostic test for the presence of Metanil Yellow at levels that can bestow an advantage to adulterers provides an incentive to develop appropriate protocols for SERS based detection. For the detection of Metanil Yellow and Malachite Green Oxalate from dals and green vegetables respectively, we used paper-based SERS strips, wetted with ethanol, to swab the skins of the dals/vegetables to enable the direct transfer of the molecules onto the silver surface. For the swabbing experiments reported here the silver nanowires (nominal silver loading of 1 MG Oxalate/cm^2) were fabricated over a circular patch with a diameter of 5 mm, which is close to the size of a single dal particle and were wetted with 20 µL of ethanol prior to swabbing. The wet SERS substrate was swabbed one time each over 3 randomly chosen dal particles and allowed to dry prior to measurement.

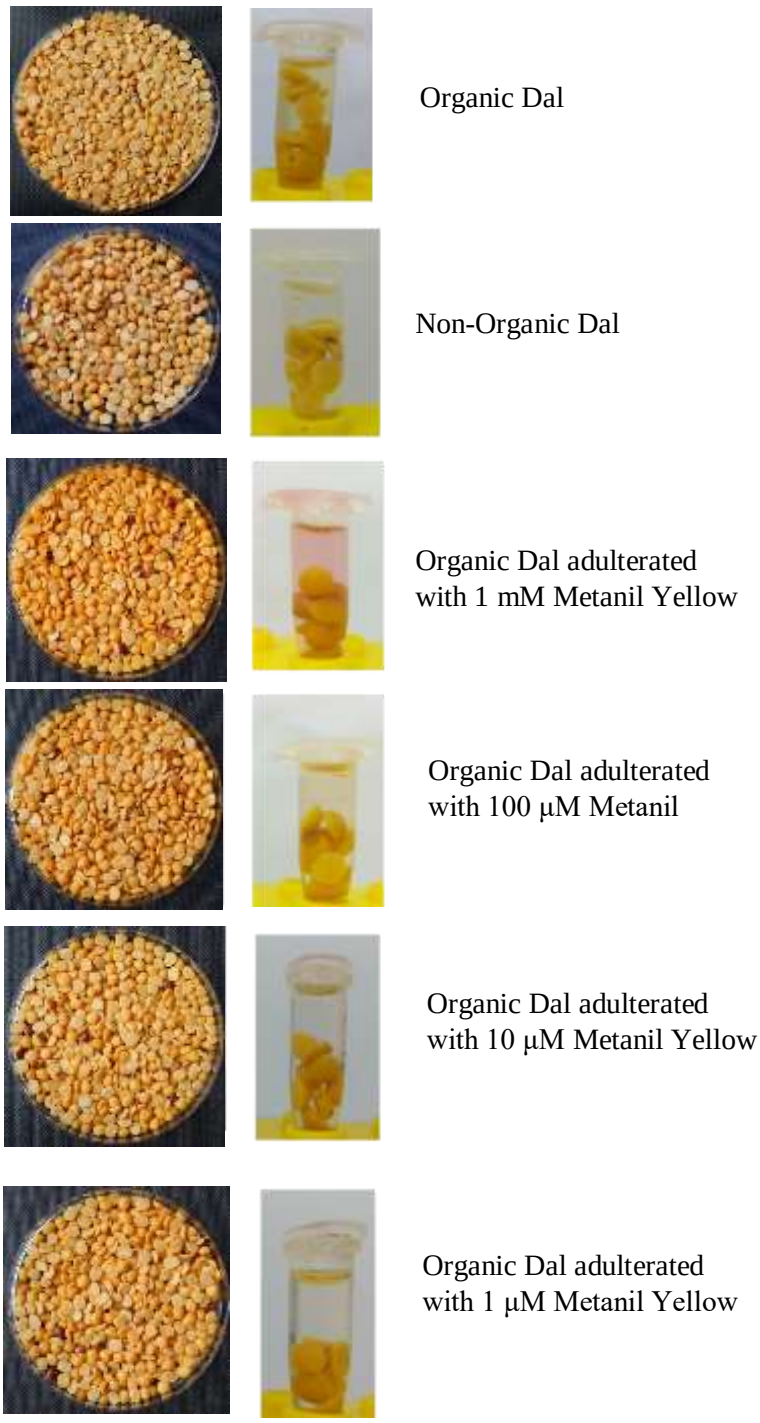

Figure 4.2 Results of FSSAI suggested HCl test for dals adulterated with Metanil Yellow. The left panels show a photograph of the dal samples, while the right panels show corresponding images of the dal samples after being immersed in a HCl solution. Comparison of adulterated dals with the non-adulterated one. Organic dal adulterated with 10 µM Metanil Yellow looks more appealing than non-adulterated dal, and organic dal adulterated with 1 mM Metanil Yellow shows the presence colour visually on comparing with the organic dal.

To test the efficacy of molecular transfer by swabbing, we carried out comparative tests by first extracting the dye into ethanol and then either drop casting the solution onto the SERS strip or dipping the SERS strip for 10 min into the solution containing the desorbed dye molecules (see Figure 4.3).

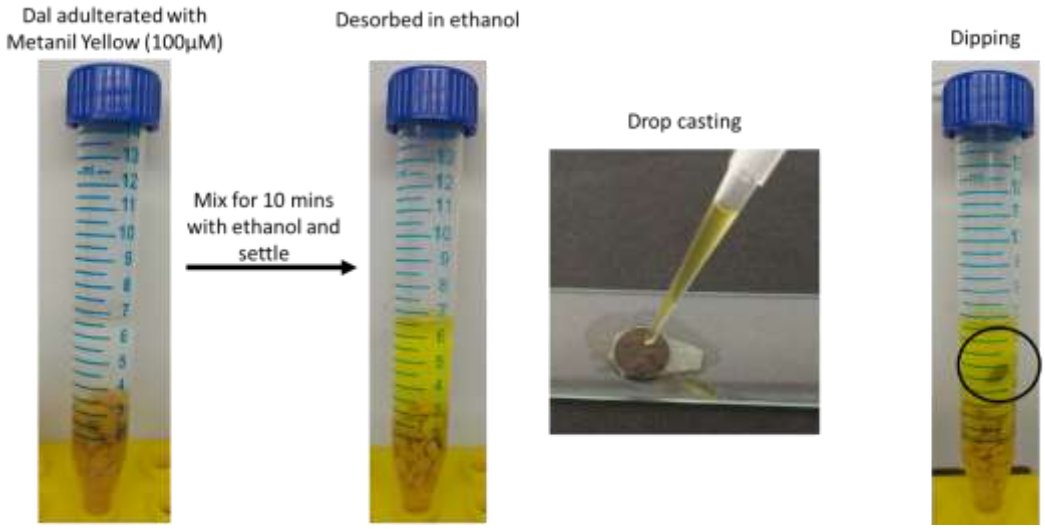

Figure 4.3 Sample Preparation techniques for SERS analysis

Figure 4.4 shows that the SERS signal from the directly swabbed sample is much higher than the drop-casted sample, while the dipped sample shows poor SERS signal. The different peaks in the SERS spectra were assigned to different moieties as per literature reports as follows ([4–7])

1193 cm^{-1} & 1437 cm^{-1} (ν(N=N)) peaks

1147 cm^{-1} (ν(C-N_{azo}) stretching)

1406 cm^{-1} (S=O stretching)

Together, these spectral peaks, specifically the presence of sulphur oxide and azo nitrogen groups) confirm the synthetic origin of these molecules and are attributed to the presence of Metanil Yellow in the test sample. The higher peak intensity of the swabbed sample attests to the efficacy of the simple swabbing protocol and highlights

the issues with dilution and dispersion of the target analyte using the more tedious solvent extraction protocol.

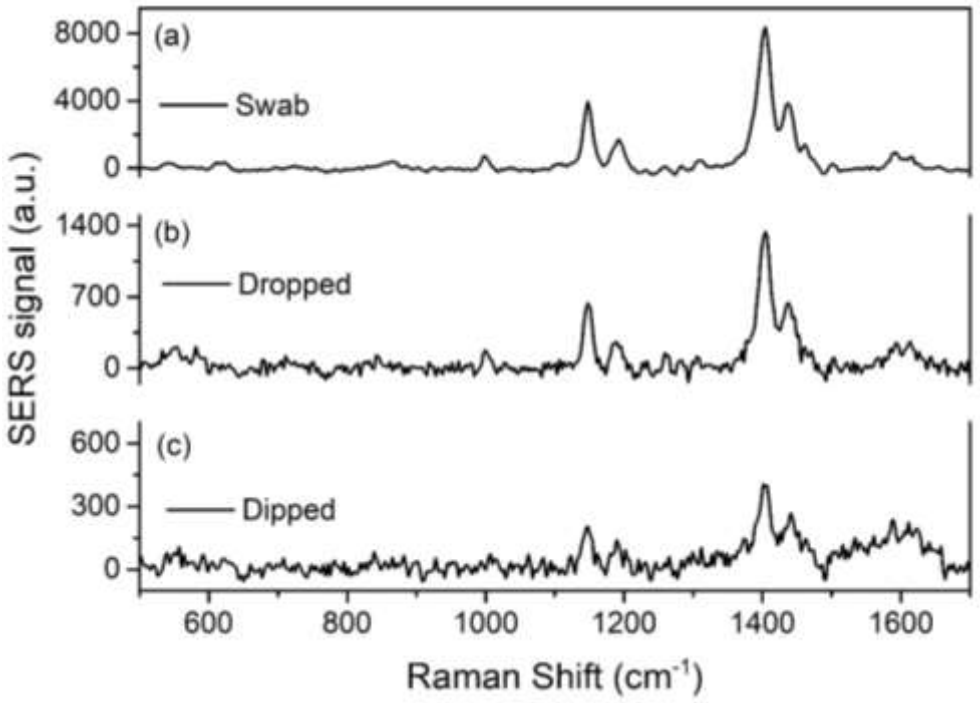

Figure 4.4 Comparison of direct swab sample with drop-cast and dipped samples. (a) SERS spectra corresponding to direct pick up of Metanil Yellow molecule from dal surface by swabbing (no desorption), (b) & (c) SERS analysis of dropped and dipped ones. SERS signals were acquired using 16.67 mW laser intensity and for integration time of 5 secs with ORS and Reference ON.

4.4 Limit of direct detection of Metanil Yellow using SERS swabs

Figure 4.5 shows the SERS spectra of swabs of intentionally-adulterated dal samples and the organic dal used as the starting material. SERS spectra of the 'Organic dal' swab is featureless which indicates that no biomolecule is leached/extracted to a significant extent by the swabbing process. SERS spectra of dal adulterated by spraying 1 mM of Metanil Yellow solution shows characteristic peaks at 1148 (ν(C-N_{azo}) stretching), 1195 (δ(C-H) bending), 1404 (S=O stretching), and 1437 cm^{-1} (ν(N=N) stretching) confirming the presence of Metanil Yellow. A similar spectrum with lower

intensity peaks is observed for the 1 µM sample and from 100 nM onwards spectra does not show the presence of any significant peak. Attempts to obtain spectra with higher signal to noise ratio using different acquisition conditions for the lower concentration samples proved futile due to excessive fluorescence background saturating the detector.

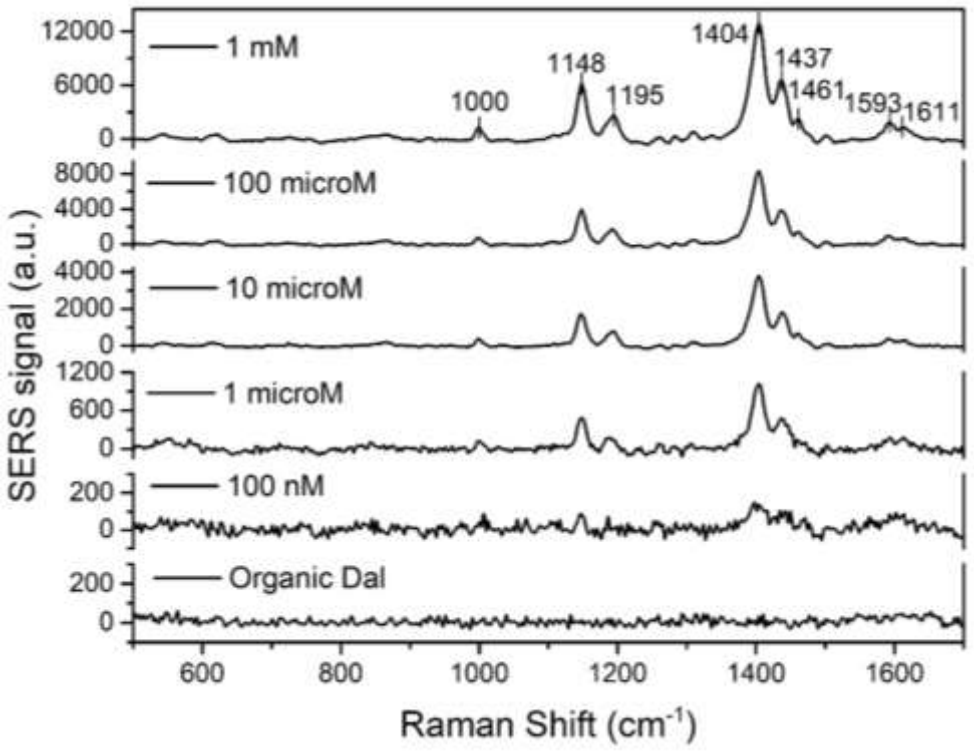

Figure 4.5 Representative SERS spectra of dal samples adulterated with Metanil Yellow. SERS signals were acquired using 16.67 mW laser intensity and integration time of 5 secs with ORS and Reference ON.

As the concentration of adulterant decreases the SERS intensity of peaks decreases, but still the spectra from the dal sample (adulterated with 1 µM of Metanil Yellow solution) has enough signal to noise ratio to identify different peaks. Therefore, SERS of swabbed samples show the capability of detecting Metanil Yellow from dal well below the concentration required for profitable use. This method does not involve any sample preparation step and onsite detection is possible using portable Raman Spectrometer.

4.5 Direct detection of Malachite Green Oxalate from green vegetables

SERS swabs were also employed for the detection of Malachite Green Oxalate from green peas and green chillies and to characterize the minimum level of detection. Samples of green peas and green chillies were thoroughly rinsed in DI water to ensure reproducibility. The 'adulterated' samples were prepared by dipping green peas and chillies into an aqueous bath of Malachite Green Oxalate for 30 min and then drying the samples overnight. For sample collection, three numbers of green peas or green chillies were wiped with SERS swabs wetted with ethanol.

SERS signal from green peas and chillies show a peak at 1370 cm^{-1}, corresponding to N-phenyl stretching (a signature group of Malachite Green Oxalate), which confirms the presence of Malachite Green Oxalate (Figure 4.6). The intensity of peaks obtained from green peas samples is lesser than that of green chillies, and this is attributed to the lower surface area of the green peas swabbed during sample collection. Figure 4.6 shows that contamination with even 100 nM solution of Malachite Green Oxalate can be easily detected. But there was no visible change in appearance (and hence no economic incentive for adulteration) of the samples dipped in Malachite Green Oxalate solutions having concentrations lower than 10 μM. Thus, direct detection using SERS swab with a portable Raman spectrometer would enable rapid and onsite detection of adulteration.

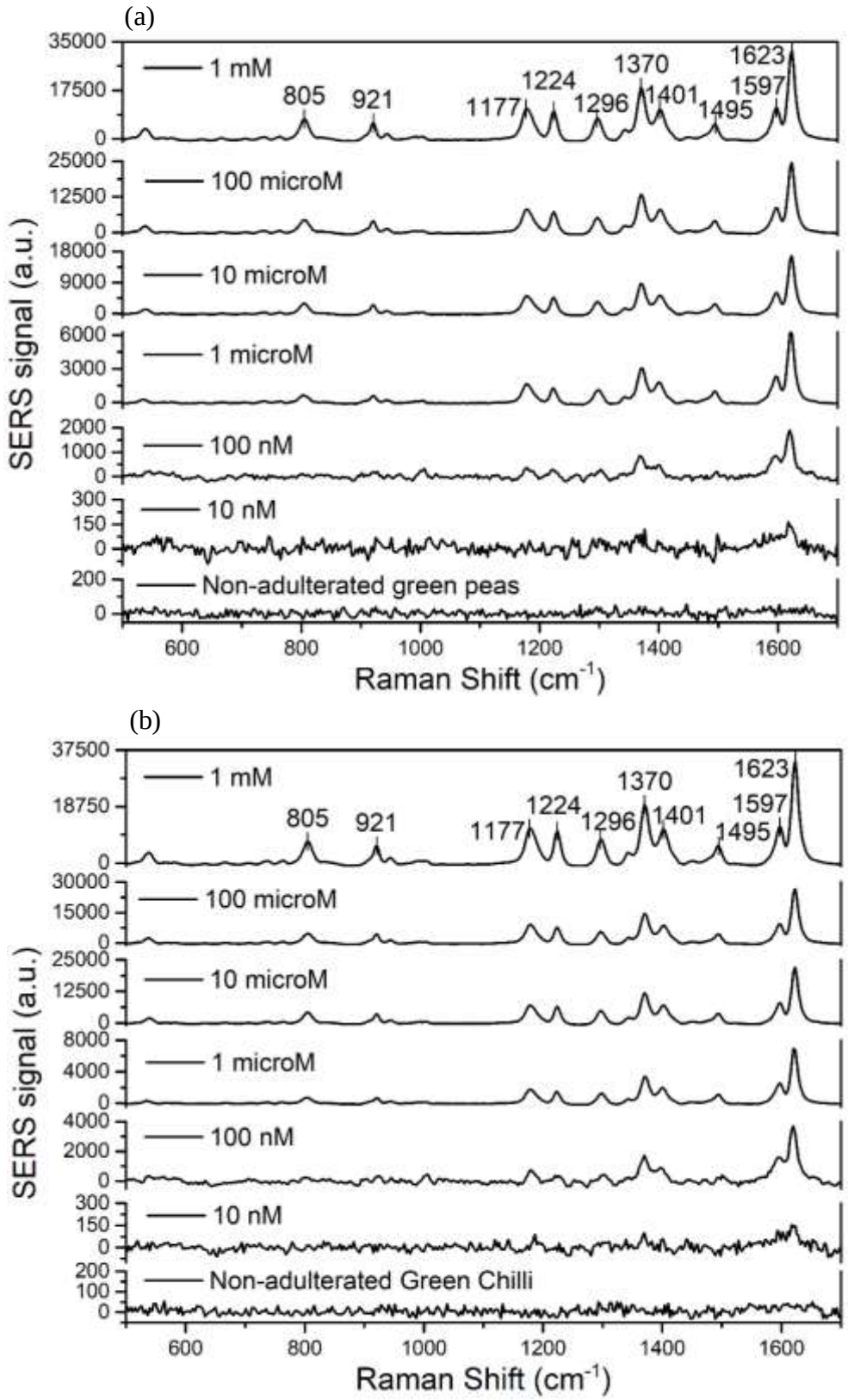

Figure 4. 6 SERS spectra of (a) Green peas, and (b) Green chillies. SERS signal acquired at 16.67 mW laser intensity and for integration time of 5 s with ORS and Reference ON.

4.6 Adulterants detection from real-world samples

Both the analysis for Metanil Yellow and Malachite Green Oxalate show the successful detection of adulterants using SERS swabs in combination with portable Raman Spectrometer. Combining SERS swabs and portable Raman Spectrometer makes it possible to achieve our objective of rapid and on-site detection with minimum sample preparation required. The samples which were used till now for either calibration of an instrument or assessing the detection limit were intentionally adulterated samples of food items. So, the next step was to employ SERS swab and portable Raman Spectrometer for testing real-world samples of dals, green peas, and green chillies. For this work, samples were collected from the local market and neighbourhood supermarkets like Reliance Fresh, around the Indian Institute of Science (IISc) Bangalore, India.

To analyse real-world samples for food adulterants, packed and open dal samples were collected from two supermarkets (Reliance Fresh and Supermarket inside IISc), and two local shops around IISc. Sample collection was performed by directly swabbing from the dal's surface with ethanol wetted SERS swab. Swabbing is done in such a way that it covers the whole surface of dal, and about three dal particles were swabbed per sample. The sample collected on the SERS swab was analysed using the portable Raman Spectrometer with optimal acquisition conditions.

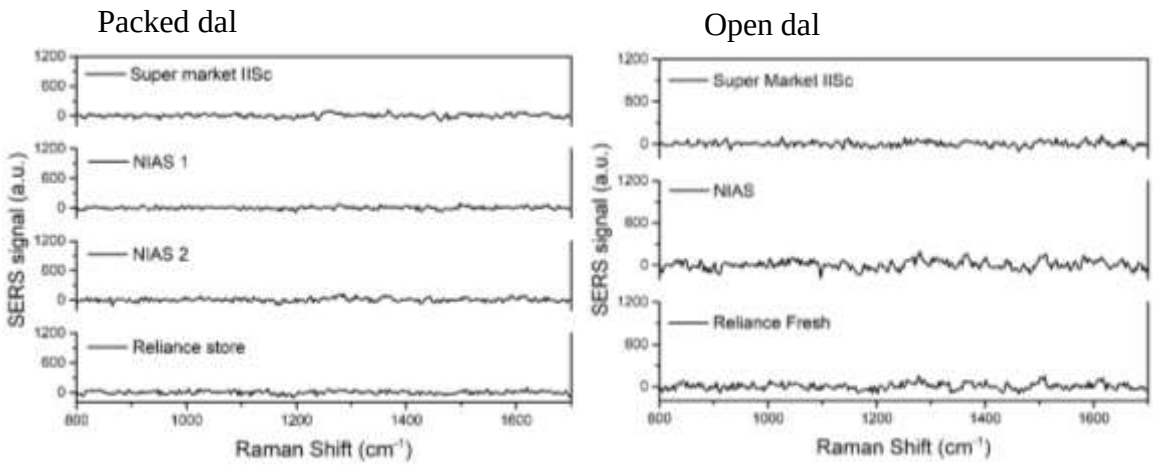

Figure 4.7 SERS spectra of different packed and open dal samples. The samples do not show any significant Raman peak confirming the absence of any foreign adulterant molecule. SERS signals were acquired using 16.67 mW laser intensity and for an integration time of 5 secs with ORS and Reference ON.

Figure 4.7 shows that the open and packed dal samples collected from shops around IISc do not show any significant peaks in their Raman spectra after swabbing. This indicates the absence of any foreign molecule on the surface of these dals. Similar analysis was performed for green peas as well as green chilly samples to check for the presence of Malachite Green Oxalate. Figure 4.8 confirms the absence of any artificial colouring on the samples of green peas and green chillies collected from stores around the IISc campus.

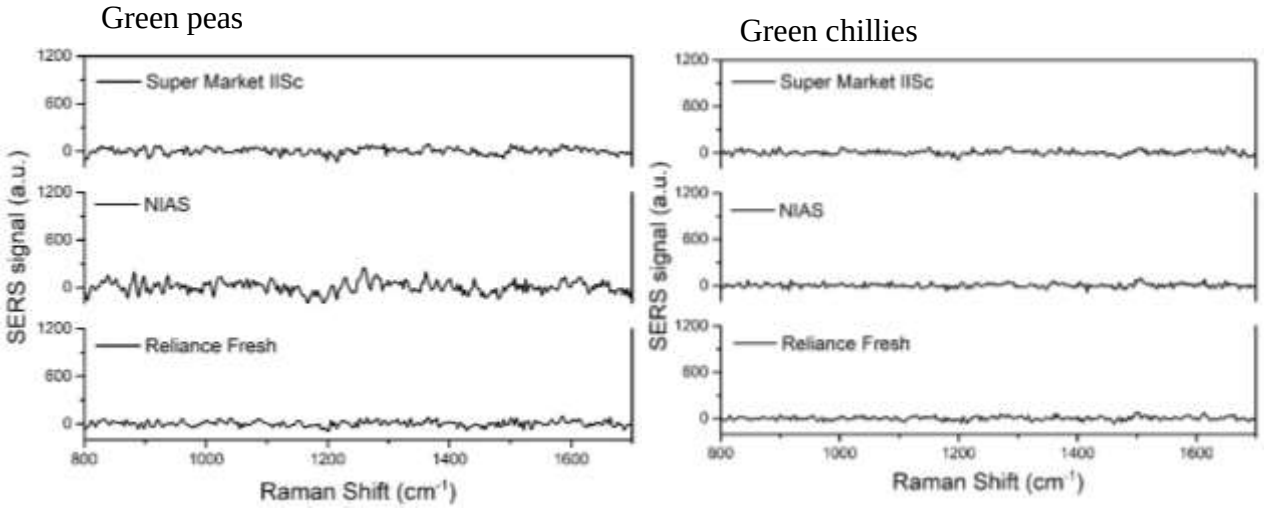

Figure 4.8 SERS spectra of green peas and green chillies from different shops around IISc. SERS spectra for both the vegetables do not show any significant Raman peak, which confirms the absence of any foreign adulterant molecule. SERS signals were acquired using 16.67 mW laser intensity and for an integration time of 5 secs with ORS and Reference ON.

Hearteningly, these preliminary analyses show the absence of any synthetic colourants in dal, green peas and green chilly samples procured from markets around IISc. But there have been alarming news and studies confirming the presence of Metanil Yellow in dals [3] and Malachite Green Oxalate in green vegetables. To explore the possibility of adulteration in the public distribution system, we solicited and received a sample of dal from a family, who procure their monthly supplies from a ration shop in Triplicane, Chennai.

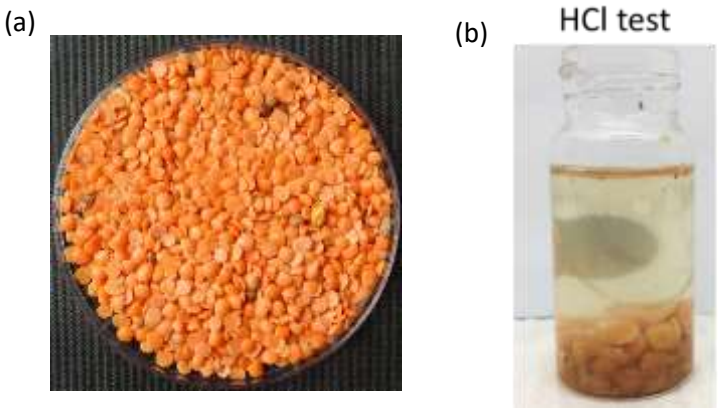

Figure 4.10 (a) Dal sample from a Ration shop in Triplicane, Chennai, (b) FSSAI suggested HCl test does not give any prink colour which is an indication of absence of Metanil Yellow.

Figure 4.9 shows a picture of the visual appearance of the dal sample as well as the results of the FSSAI-suggested quick diagnostic test for Metanil Yellow. Although the sample appears to be uniformly coloured, the FSSAI test results were negative. We directly swabbed the sample with a SERS swab that was wet with ethanol and obtained its SERS spectrum using the portable Raman spectrometer. Figure 4.10 clearly shows the tell-tale signature of Metanil Yellow with all the four major peaks 1148 (ν(C-N_{azo}) stretching), 1193 (δ(C-H) bending), 1404 (S=O stretching) and 1438 cm^{-1} (ν(N=N) stretching) being present. This result unambiguously proves the applicability of paper-based SERS swabs for rapid onsite detection of adulteration of food samples.

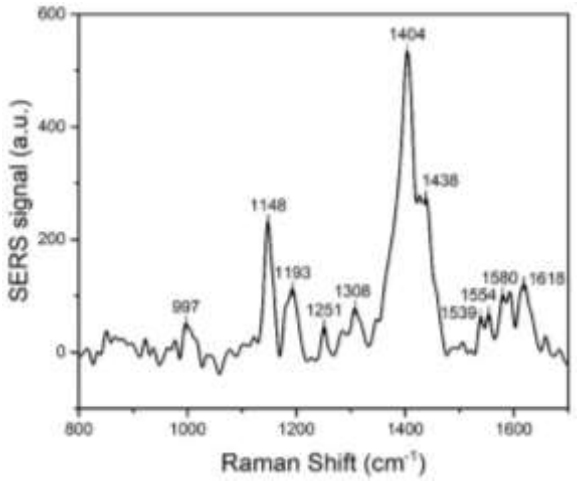

Figure 4.9 SERS spectra of dal from a ration shop in Chennai showing major peaks related to Metanil Yellow. SERS signal was acquired at 16.67 mW laser intensity and for integration time of 5 secs with ORS and Reference ON.

4.7 Adulterant removal capability of cleaning solutions available in the market

Till now, this work has shown the detection capability of adulterants using SERS swabs and portable Raman Spectrometer. Several companies have introduced either soap-based cleaners or 'ozoniser' based cleaners for vegetables and fruits to capitalize on the widespread anxiety in the minds of people about unknown adulterants on food items. So, SERS analysis of knowingly adulterated green peas and/or green chilly samples before and after cleaning was performed to test the removal capability of these cleaners. The percentage decrease in the SERS signal after washing in comparison to that before washing was quantified for the several cleaning solutions available in the market. We performed a series of experiments to verify the efficacy of these 'cleaning solutions' *vis a vis* standard protocols used in most households. These include:

1) Rinsing with tap water (the most common method used in every household to clean food items)
2) Washing with cleaners and then rinsing with tap water
3) Cleaning with ozoniser

4.7.1 Rinsing with tap water

In every household, to clean vegetables rinsing with tap water is typically done with an expectation that it will remove dirt and water-soluble adulterants which may be present on the vegetables. So, SERS spectra of green peas swabbed before and after rinsing with tap water were measured (Figure 4.11). For the analysis, 'adulterated' green peas sample was prepared by dipping green peas in 100 µM solution of Malachite Green Oxalate dye for 30 min and then allowing it to dry overnight in the laboratory. The reduction in the integrated area of peak at 1372 cm^{-1} (N-phenyl stretching) indicates ~35% removal of Malachite Green Oxalate was achieved just by rinsing with tap water.

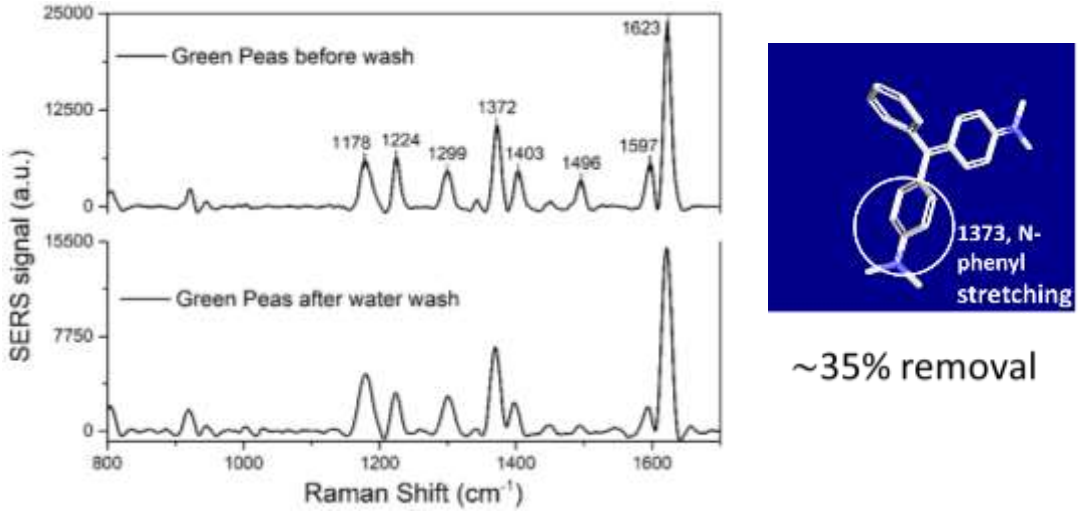

Figure 4.11 SERS spectra from swab of green peas before and after rinsing with tap water show 35% reduction in the integrated peak area of 1372 cm^{-1} peak. SERS spectra are collected at 16.67 mW laser power with an integration time of 5 s with ORS and Reference ON.

4.7.2 Direct washing with cleaners

Additionally, a detailed set of experiments were performed on both green peas as well as green chillies for ascertaining the cleaning capability of commercially available products, when used as per the directions provided by the manufacturer. The adulterated samples were prepared by dipping organic produce in 100 µM solution of Malachite Green Oxalate dye for 30 min and then allowing them to dry overnight in the laboratory. For the removal of adulterants from green peas and chillies, three different brands of cleaners have been employed in this analysis. After using the cleaners, the vegetables were rinsed with tap water.

As shown in Figure 4.13, after washing with cleaners (Figure 4.12), peaks corresponding to Malachite Green Oxalate are still present in the SERS spectra of the swabbed samples. Typically, 60- 70% reduction in the signal at 1372 cm^{-1} was obtained, indicating that a significant amount of dye is left on the skins of these vegetables even after washing. Notably, there were no additional residues due to the use of the cleaning solutions.

Figure 4.12 Photographs of different cleaners used.

4.7.3 Cleaning with ozoniser

To detoxify the fruits and vegetables some companies have introduced table top cleaners/ 'ozoniser' which purport to use ozone technology to sterilize the fruit and vegetables and make them fit for consumption. The typical ozone output from these ozonisers is 200 mg/h. For our analysis, we procured a generic ozoniser with double the ozone output, 400 mg/h from an online vendor. Ozonisation was performed for 15 mins on adulterated green chillies, which is enough time for removal of toxic chemicals as claimed by the manufacturer. SERS spectra were obtained by swabbing some of the samples after 'ozonising' and compared with the signal obtained prior to cleaning. After 15 min of ozonisation, reduction in the integrated area of peak at 1373 cm^{-1} was found to be 88%, which shows 88 % removal of Malachite Green Oxalate from the green chillies (Figure 4.14).

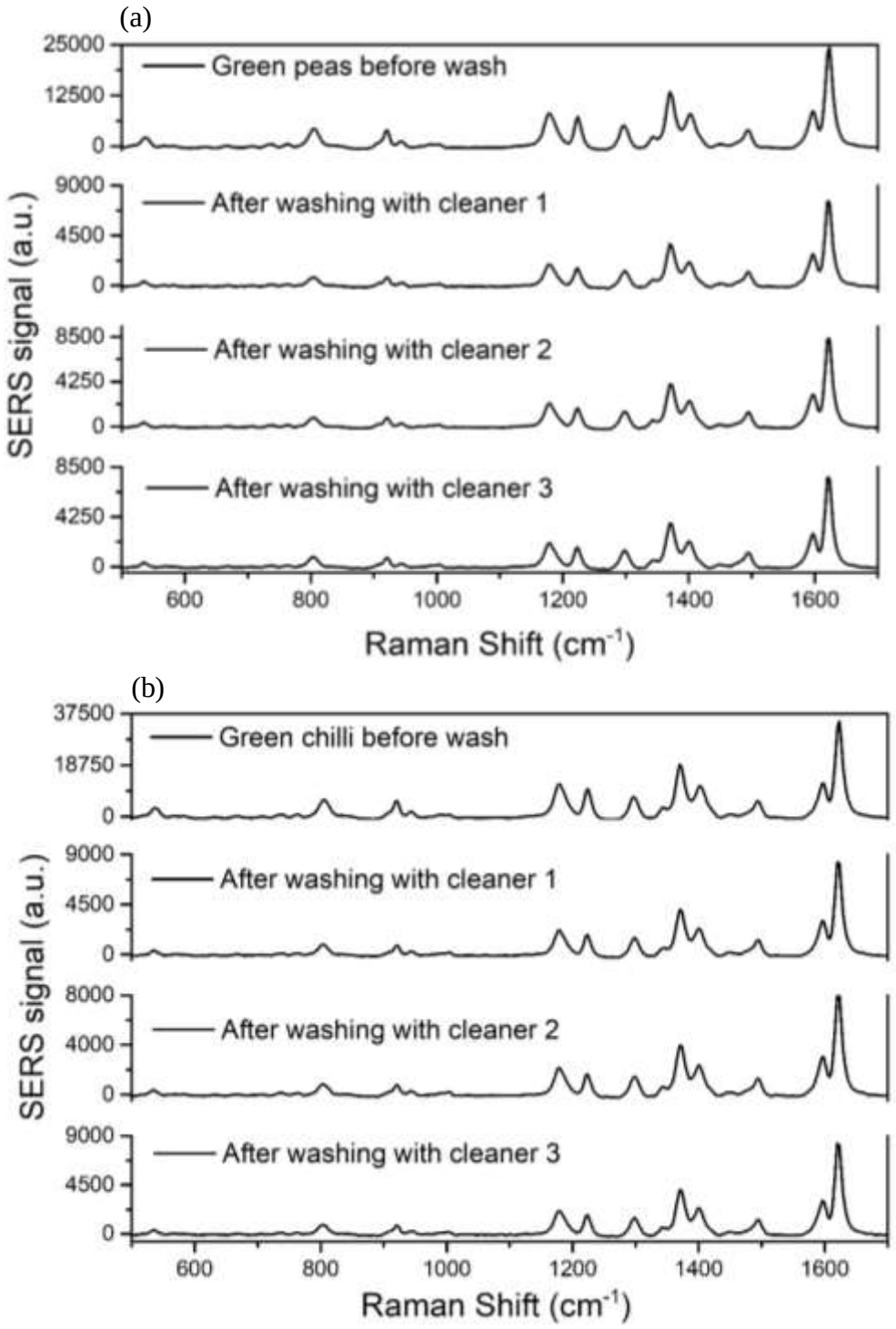

Figure 4.13 SERS spectra of (a) green peas, and (b) green chilli before and after washing with three different brands of detoxifying cleaners. Average removal capability of all the cleaners range from 60-70%. SERS spectra are collected at 16.67 mW laser power with an integration time of 5 s with ORS and Reference ON.

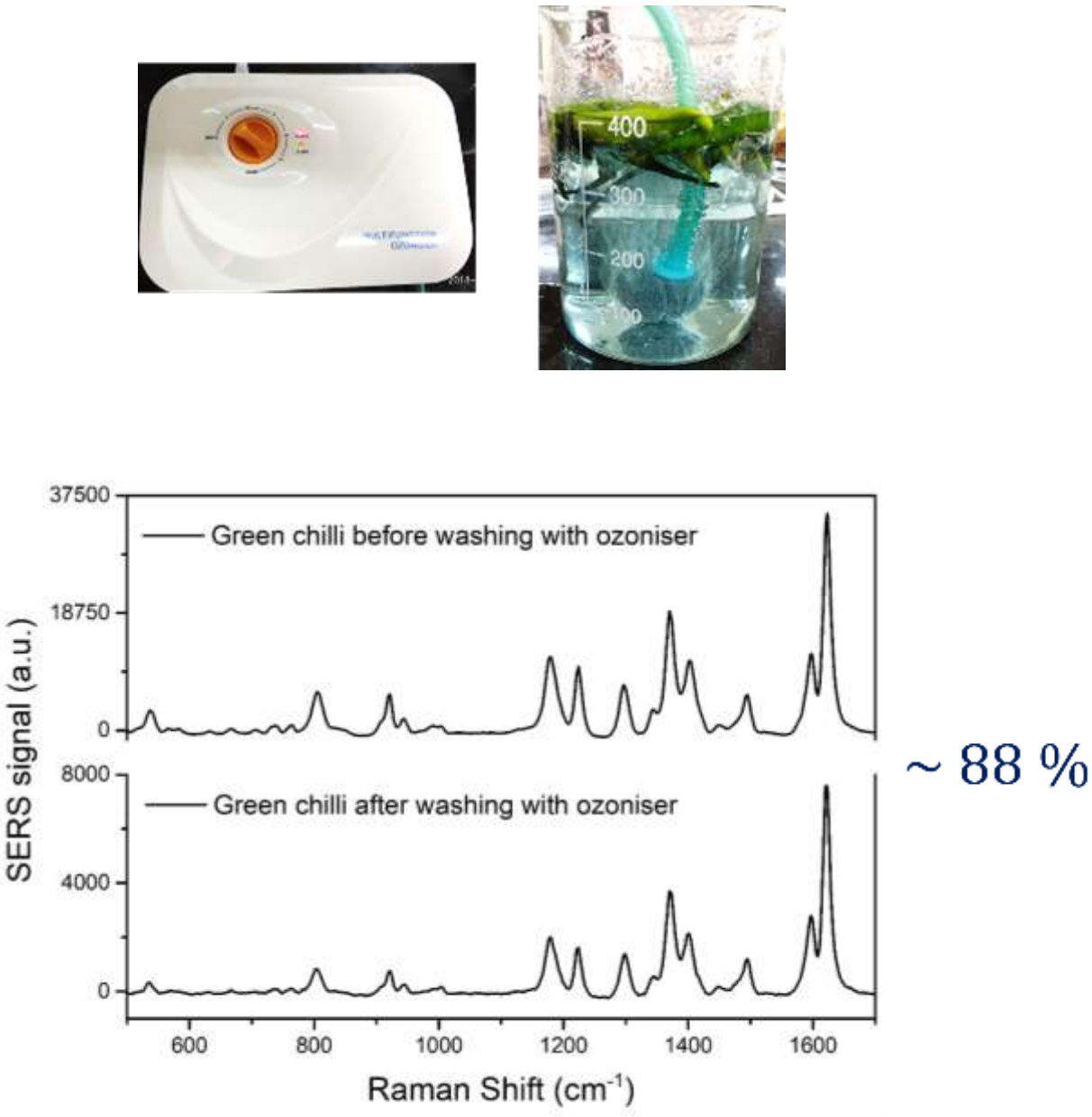

Figure 4.14 Top – A photograph of the ozoniser and the setup used for ozonisation. Bottom - SERS spectra from swabs of green chillies before and after the ozonisation. Even after ozonisation Malachite Green Oxalate peaks, albeit at a lower intensity, are still present, which shows the presence of dye even after ozonisation. SERS spectra were collected at 16.67 mW

4.8 Summary

To summarize, this chapter explores the use of SERS swab and portable Raman Spectrometer for the detection of Metanil Yellow and Malachite Green Oxalate on dals and green vegetables respectively. First, we analysed Metanil Yellow using the FSSAI suggested HCl test and found that the limit of detection was not appropriate enough to identify adulteration in the marketplace. Swabbing using paper-based SERS strips was found to be best for detecting adulterants from the skins of vegetables and dals. The limits of detection were determined to be 1 μM for Metanil Yellow on dals and 100 nM of Malachite Green Oxalate on green vegetables. SERS swabs were also found to be suitable for detecting adulteration on real-world samples of dals and green vegetables, and easily identified the presence of Metanil Yellow on dal from a ration shop, even when the FSSAI suggested quick diagnostic test failed to detect the presence of Metanil Yellow. Further, we tested several cleaning solutions available in the marketplace and found that none of them can remove close to 100% of the dye molecules from the skins of vegetables, as claimed by the manufacturers. Albeit, these solutions were better than just rinsing in tap water.

REFERENCES

[1] M. Tripathi, S.K. Khanna, M. Das, Surveillance on use of synthetic colours in eatables vis a vis Prevention of Food Adulteration Act of India, Food Control. 18 (2007) 211–219. doi:10.1016/J.FOODCONT.2005.09.016.

[2] DownToEarth, Rampant food adulteration in Mysore, (2015). https://www.downtoearth.org.in/news/rampant-food-adulteration-in-mysore-4576 (accessed July 30, 2018).

[3] B. V Sudheer, M.K. Lakshmidevi, D. V Krishna Rao, Adulteration of the pulses in coastal region of Andhra Pradesh, J Evol. Med Dent Sci J. Evol. Med. Dent. Sci. 4 (2015) 6187–6192. doi:10.14260/jemds/2015/902.

[4] S. Dhakal, K. Chao, W. Schmidt, J. Qin, M. Kim, D. Chan, Evaluation of Turmeric Powder Adulterated with Metanil Yellow Using FT-Raman and FT-IR Spectroscopy., Foods (Basel, Switzerland). 5 (2016). doi:10.3390/foods5020036.

[5] N. Mainreck, S. Brézillon, G.D. Sockalingum, F.-X. Maquart, M. Manfait, Y. Wegrowski, Rapid Characterization of Glycosaminoglycans Using a Combined Approach by Infrared and Raman Microspectroscopies, J. Pharm. Sci. 100 (2011) 441–450. doi:10.1002/JPS.22288.

[6] O. Yamada, H. Hiura, T. Igarashi, N. Kaneko, H. Takahashi, Configuration-sensitive infrared bands and vibrational assignments of S-alkyldithizones based on isotopic substitutions, Spectrochim. Acta Part A Mol. Spectrosc. 44 (1988) 1409–1415. doi:10.1016/0584-8539(88)80191-0.

[7] P. Sett, A.K. De, S. Chattopadhyay, P.K. Mallick, Raman excitation profile of diphenylamine, Chem. Phys. 276 (2002) 211–224. doi:10.1016/S0301-0104(01)00571-7.

Chapter 5 Summary and future scope

5.1 Summary and conclusion

Use of adulterants and pesticides in food products is a cause for concern because of their adverse effects on human health. To make food items appear fresh and appealing or to improve the shelf life of fruits and vegetables, adulterants are used. For the detection of adulterants, conventional methods which are employed are time-consuming and complex processes. The entire process from collection of foods to the final report, it takes 1-2-week time which makes it impossible to take preventive steps to stop the inflow of adulterated food items in the market. This thesis presents an alternate fast detection method which takes a few minutes to give results. The alternate method involves the use of inkjet printed SERS substrates on Kimwipe tissue paper and portable Raman Spectrometer. Due to the portability of SERS substrate and Raman Spectrometer, onsite detection is possible which makes it feasible to stop the inflow of adulterated food items in the market.

For the fabrication of SERS substrate, a desktop inkjet printer is used to generate silver nanostructures on Kimwipe tissue paper, with the chemistry based on silver halide photography. For the detection of adulterants, portable Raman Spectrometer is used instead of confocal Raman Spectrometer for enabling onsite and rapid detection by swabbing the food surface using SERS swab to pick target molecules.

SERS signal variation across substrates with a nominal silver loading of 1 mg/cm^2 was found to be 1.6%. This robust response despite the microscale non-uniformity of the silver nanostructures and surface roughness of the paper substrate is attributed to the larger interrogation areas (~2 mm diameter) using ORS technology.

Further to test the detection capability of portable Raman Spectrometer, the adsorption-analysis was performed. Rhodamine 6G could be detected upto pM range, while Malachite Green and Metanil Yellow could be detected upto nM range. The difference

in sensitivity is attributed to the Resonant Raman effect in the case of R6G using a 532 nm laser source.

For the real-time application of SERS swab method, it is compared with the FSSAI suggested test for the detection of Metanil Yellow from dals and Malachite Green from green vegetables. The analysis shows that the SERS swab method can detect adulterants well below the detection limit of FSSAI suggested tests. Real world samples of dals and green vegetables around IISc were examined for adulterants presence and SERS swab test were negative, which confirms the absence of Metanil Yellow in dals and Malachite Green in green vegetables around IISc. A dal sample from a ration shop in Triplicane, Chennai was as found to be adulterated with Metanil Yellow.

Removal capability of market available cleaners and ozoniser was also tested with respect to the reduction in the integrated area of signature peaks in SERS spectra. Results show that it is possible to remove around 60-75% of the adulterants using liquid-based cleaners and around 88% with an ozoniser.

5.2 Future scope

Food items are not only adulterated with synthetic colours but also with different kind of pesticides. Many studies have shown the successful detection of pesticides from food items using SERS substrates and confocal Raman Spectroscopy. To highlight the challenges in using SERS swabs for pesticide detcetion from real world samples, spectra of a dichlorvos liquid formulation was acquired (Figure 5.1).

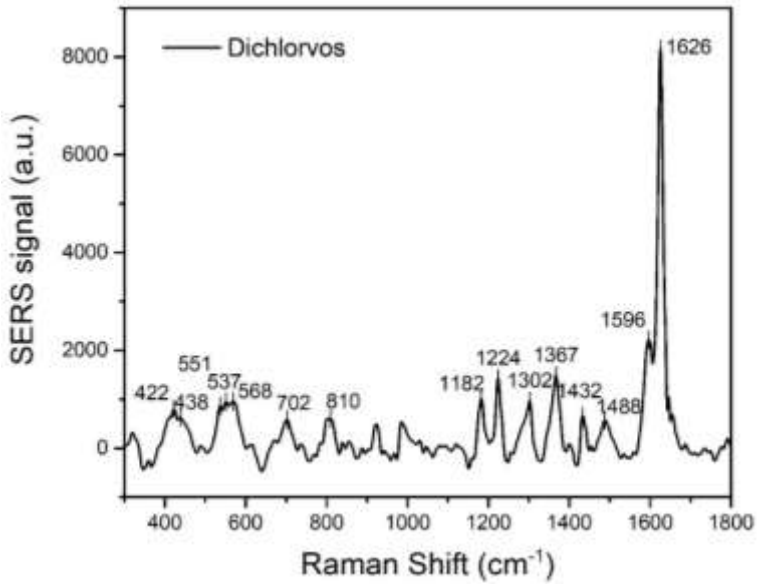

Figure 5.1 SERS spectra of neat dichlorvos liquid from dropcasting 10 µL of pesticide formulation (76% EC, diluted 25x) in water on Kimwipe SERS substrate. SERS signal was acquired using 20 mW laser intensity and integration time of 5 secs with ORS and Reference ON.

The peak with the largest intensity at 1626 cm^{-1}, corresponding to phenyl stretches is because of additional formulating agents as the active ingredient, dichlorvos, is a linear chain molecule. The detection of the presence of dichlorvos residue becomes challenging without separation from the other molecules present in the matrix. Paper-chromatographic techniques represent an attractive avenue to perform on-site separation and detection. The protocols required for carrying out such separations and enabling only the active-ingredient to reach the parts of the paper coated with SERS active nanostructures needs to be investigated.

Appendix A- Adsorption analysis data

A.1 Rhodamine 6G dye

SERS spectra of Rhodamine 6G dye was collected by soaking Kimwipe SERS substrate in aqueous solutions having desired concentration of R6G for 12 hrs, followed by rinsing with DI water to remove trace of physically adsorbed dye molecules.

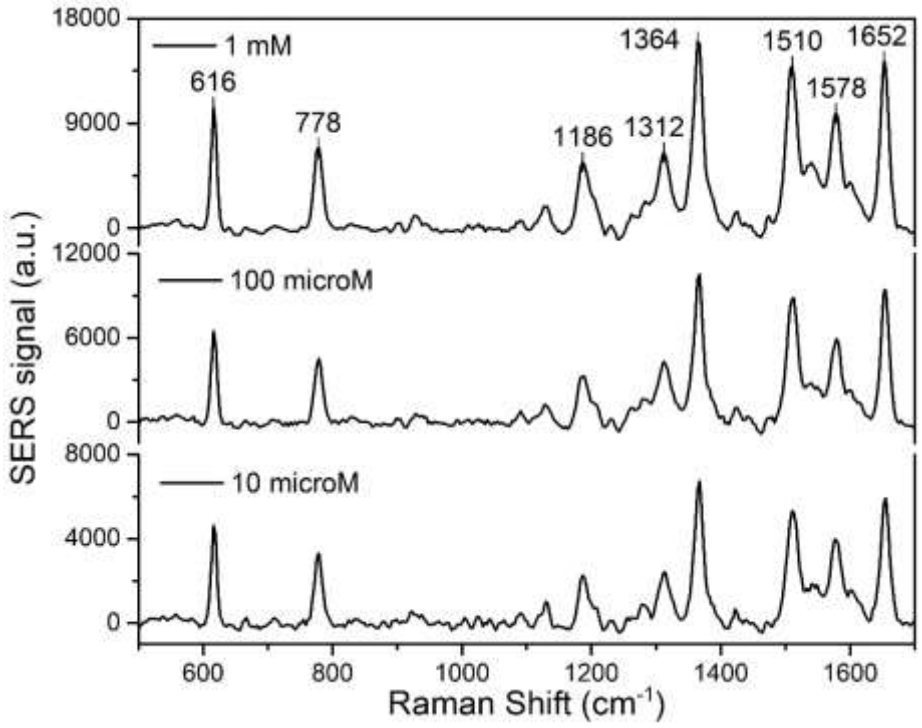

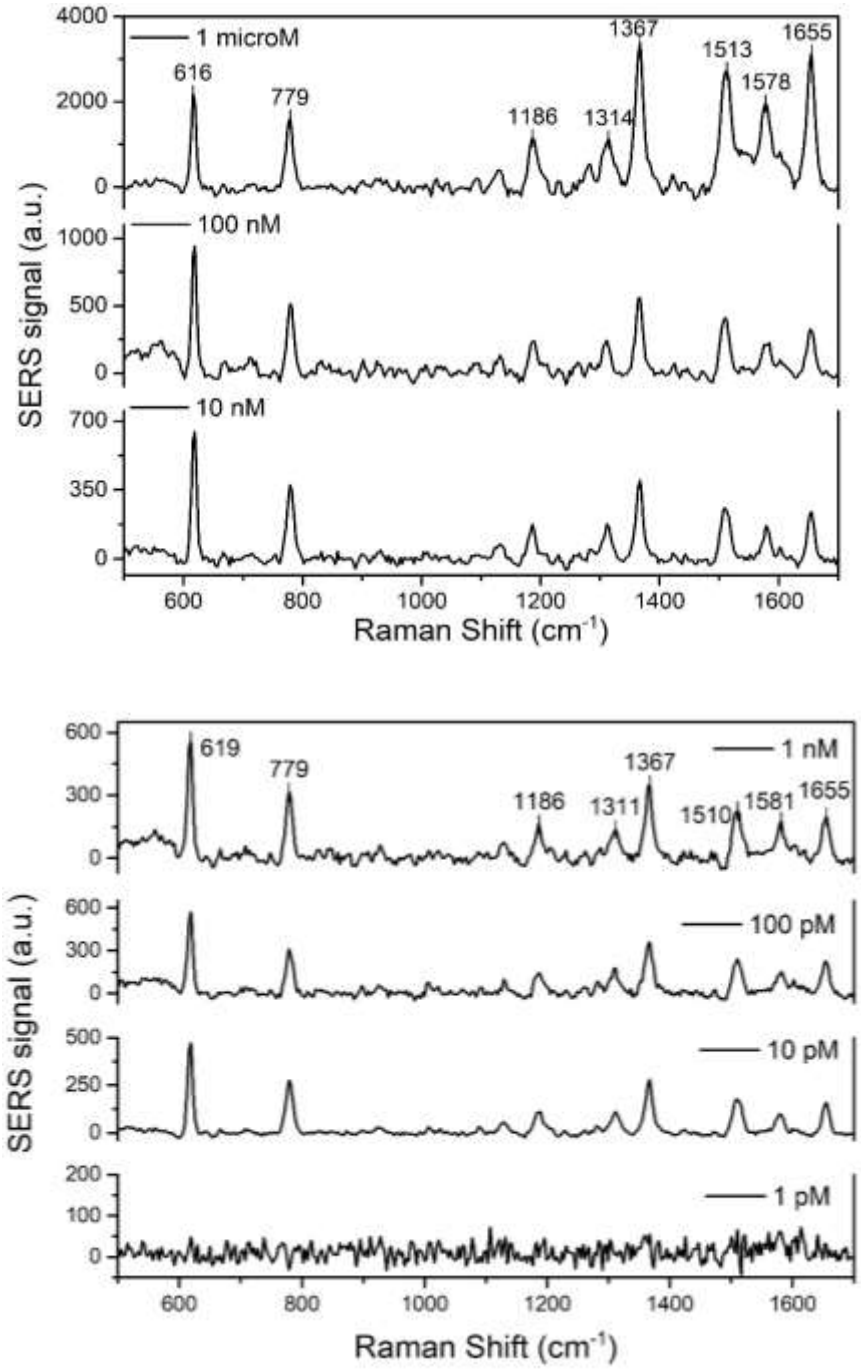

Figure A.1 Representative SERS spectra of R6G dye adsorbed onto Kimwipe silver nanostructured substrate. Concentration of R6G solution varies from 1 mM to 1 pM. Spectra were acquired using 3.33 mW laser power and 1 s integration time with ORS and Reference ON conditions.

A.2 Malachite Green Oxalate dye

The substrates were soaked in aqueous solutions having desired concentration of MG Oxalate for 12 hrs and then rinsed with DI water to remove trace of physically adsorbed MG Oxalate molecules.

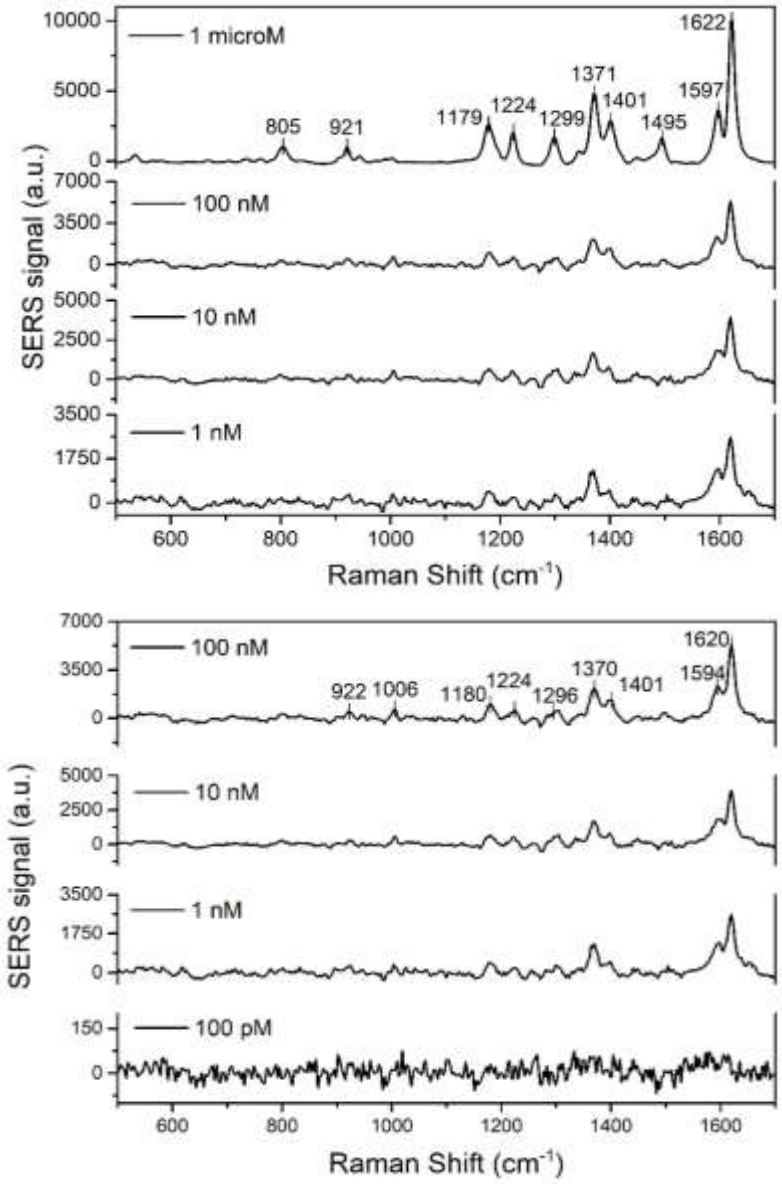

Figure A.2 Representative SERS spectra of MG Oxalate dye adsorbed onto Kimwipe silver nanostructured substrate. Concentration of solution varies from 1 mM to 100 pM. Spectra were acquired using 16.67 mW laser power and 5 s integration time with ORS and Reference ON conditions.

A.3 Metanil Yellow dye

Paper-based SERS substrates were soaked in aqueous solutions having desired concentration of MY for 12 hrs and then rinsed with DI water.

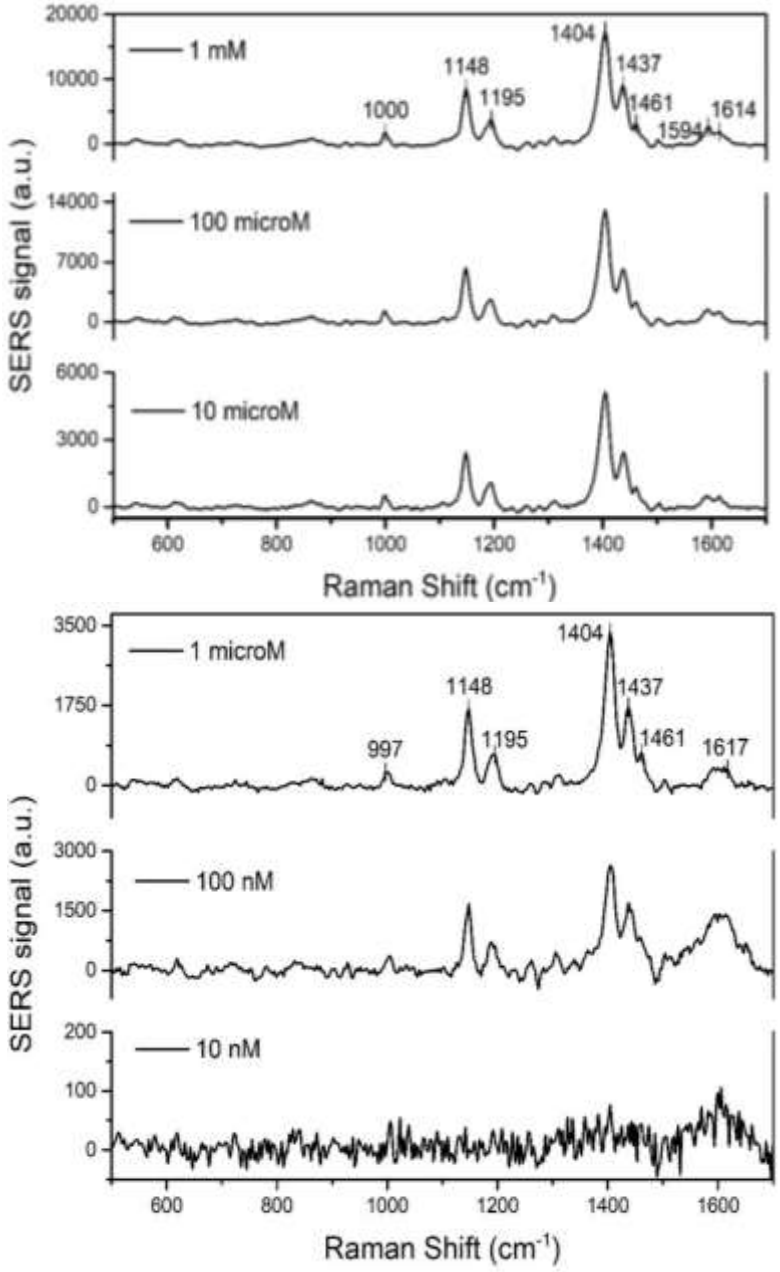

Figure A.3 Representative SERS spectra of MY dye adsorbed onto Kimwipe silver nanostructured substrate. Concentration of solution varies from 1 mM to 10 nM. Spectra were acquired using 16.67 mW laser power and 5 s integration time with ORS and Reference ON conditions.

Appendix B- Data Processing with ORIGIN software

Data processing for subtracting the fluorescence background and denoising the spectra was done using ORIGIN-Graphing and data analysis software. The illustration of background correction of R6G adsorbed onto Kimwipe tissue paper.

Raw Data

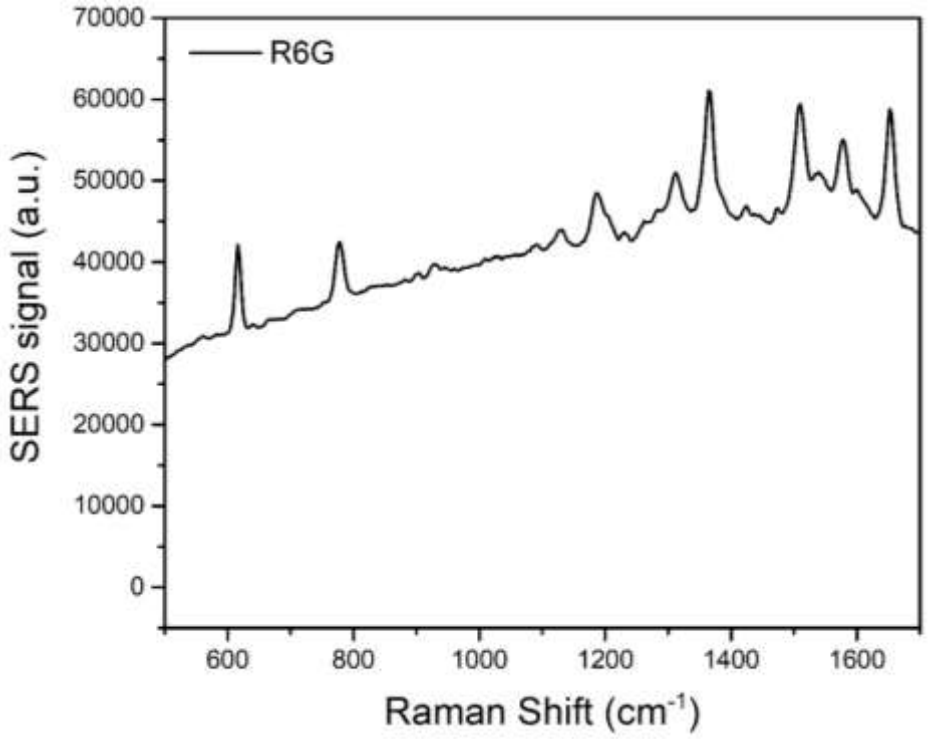

Background correction steps

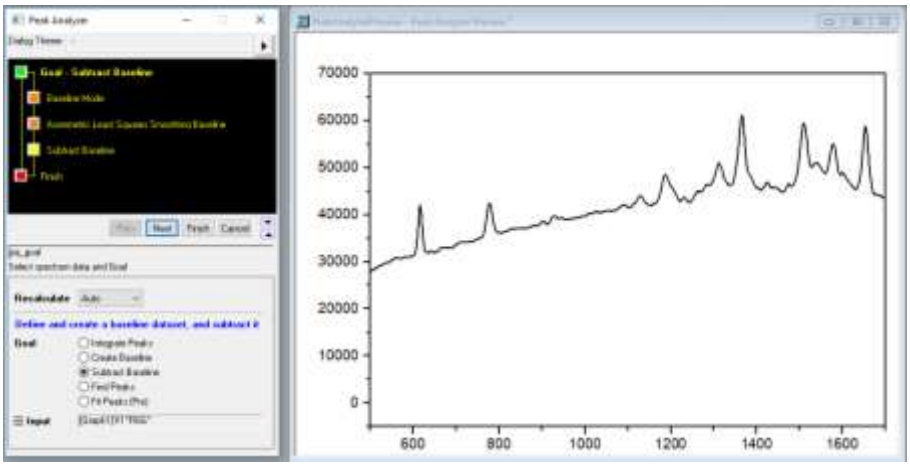

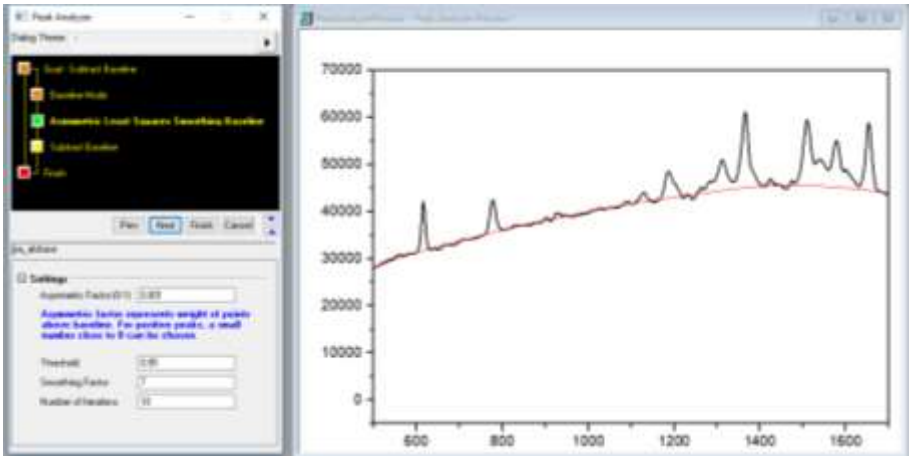

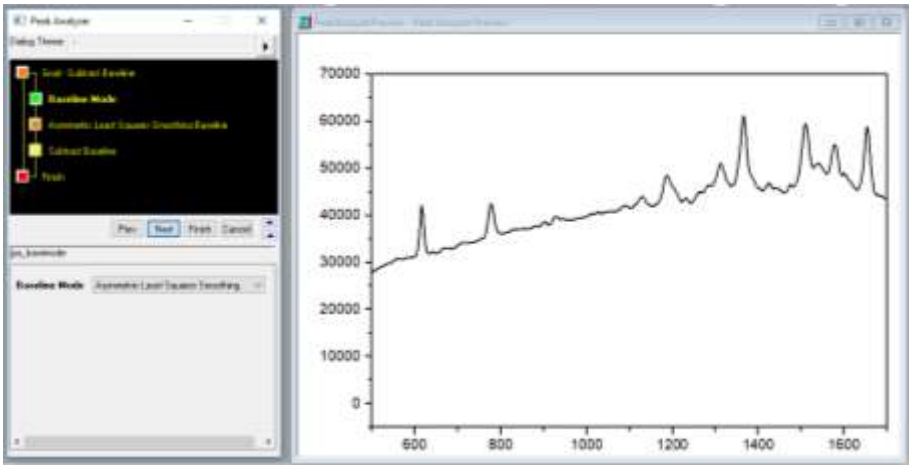

Background corrected spectrum

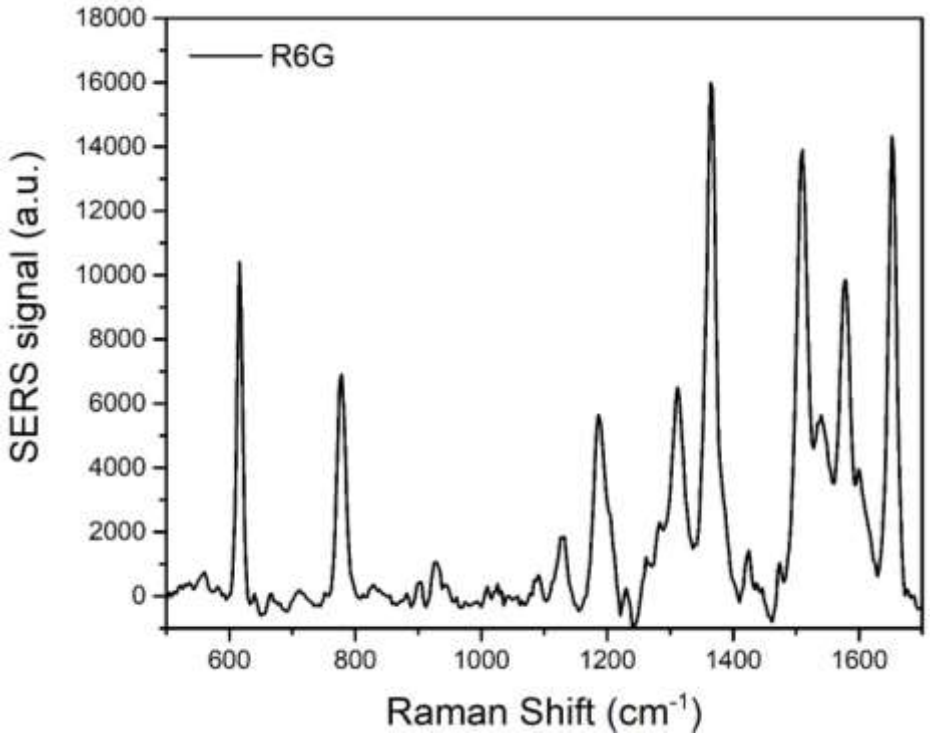

Denoising spectrum using wavelet transform

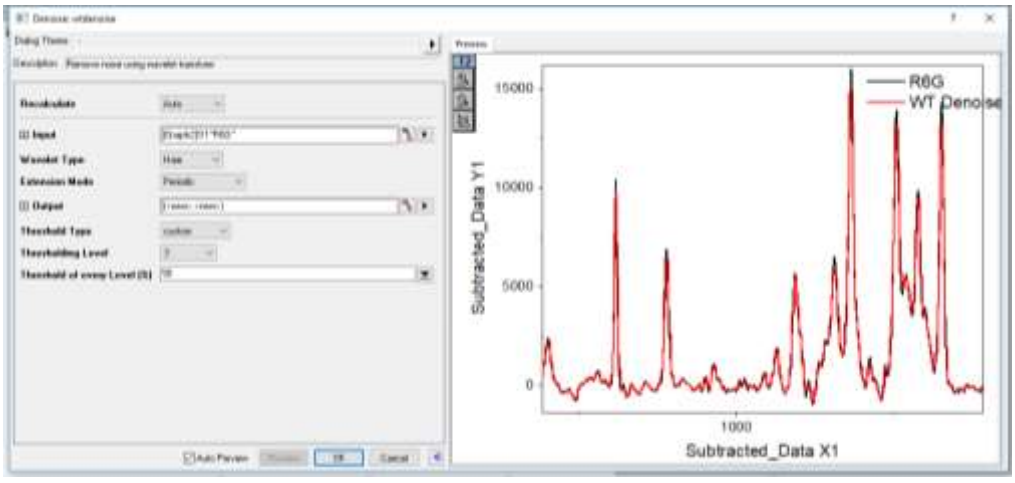

Denoised spectrum